

## Review

**Cite this article:** Frykholm K, Müller V, KK S, Dorfman KD, Westerlund F (2022). DNA in nanochannels: theory and applications. *Quarterly Reviews of Biophysics* **55**, e12, 1–27. <https://doi.org/10.1017/S0033583522000117>

Received: 16 May 2022  
Revised: 30 September 2022  
Accepted: 4 October 2022

### Key words:


DNA; nanofluidics; optical DNA mapping; polymer physics; single molecules

### Author for correspondence:

Fredrik Westerlund,  
E-mail: [fredrikw@chalmers.se](mailto:fredrikw@chalmers.se)

© The Author(s), 2022. Published by Cambridge University Press. This is an Open Access article, distributed under the terms of the Creative Commons Attribution licence (<http://creativecommons.org/licenses/by/4.0/>), which permits unrestricted re-use, distribution and reproduction, provided the original article is properly cited.

# DNA in nanochannels: theory and applications

Karolin Frykholm<sup>1</sup>, Vilhelm Müller<sup>1</sup>, Sriram KK<sup>1</sup>, Kevin D. Dorfman<sup>2</sup>  
and Fredrik Westerlund<sup>1</sup> 

<sup>1</sup>Department of Biology and Biological Engineering, Chalmers University of Technology, Kemivägen 10, 412 96 Gothenburg, Sweden and <sup>2</sup>Department of Chemical Engineering and Materials Science, University of Minnesota, Minneapolis, MN 55455-0132, USA

## Abstract

Nanofluidic structures have over the last two decades emerged as a powerful platform for detailed analysis of DNA on the kilobase pair length scale. When DNA is confined to a nanochannel, the combination of excluded volume and DNA stiffness leads to the DNA being stretched to near its full contour length. Importantly, this stretching takes place at equilibrium, without any chemical modifications to the DNA. As a result, any DNA can be analyzed, such as DNA extracted from cells or circular DNA, and it is straight-forward to study reactions on the ends of linear DNA. In this comprehensive review, we first give a thorough description of the current understanding of the polymer physics of DNA and how that leads to stretching in nanochannels. We then describe how the versatility of nanofabrication can be used to design devices specifically tailored for the problem at hand, either by controlling the degree of confinement or enabling facile exchange of reagents to measure DNA–protein reaction kinetics. The remainder of the review focuses on two important applications of confining DNA in nanochannels. The first is optical DNA mapping, which provides the genomic sequence of intact DNA molecules in excess of 100 kilobase pairs in size, with kilobase pair resolution, through labeling strategies that are suitable for fluorescence microscopy. In this section, we highlight solutions to the technical aspects of genomic mapping, including the use of enzyme-based labeling and affinity-based labeling to produce the genomic maps, rather than recent applications in human genetics. The second is DNA–protein interactions, and several recent examples of such studies on DNA compaction, filamentous protein complexes, and reactions with DNA ends are presented. Taken together, these two applications demonstrate the power of DNA confinement and nanofluidics in genomics, molecular biology, and biophysics.

## Table of contents

<b>Introduction</b>	<b>1</b>
<b>Theory</b>	<b>2</b>
Length scales characterizing DNA in free solution	2
Configuration of DNA in channel confinement	4
Effects of crowding agents	9
Outstanding challenges	9
<b>Devices</b>	<b>10</b>
Fabrication processes	10
Chip designs	10
CLiC (Convex Lens-induced Confinement)	13
Passivation	13
<b>Optical DNA mapping</b>	<b>13</b>
Enzyme-based labeling	14
Affinity-based labeling	14
Recent applications of optical DNA mapping	15
Outstanding challenges	16
<b>DNA–protein interactions</b>	<b>16</b>
DNA compacting proteins	16
Filamentous DNA–protein complexes	19
Proteins interacting with DNA ends	20
Other DNA–protein interactions	21
Outstanding challenges	22
<b>Summary</b>	<b>22</b>

## Introduction

Methods to study single DNA molecules have revolutionized science across disciplines, ranging from fundamental biophysics to clinical diagnostics. The possibility to interrogate single DNA molecules enables information that is intrinsically hidden in bulk experiments to be obtained in a straight-forward fashion. Focusing on DNA molecules with a length in the kilobase pair (kbp) regime, traditional methods include for example optical (Chaurasiya *et al.*, 2010; Heller *et al.*, 2014) and magnetic (De Vlaminck and Dekker, 2012) tweezers, where a single DNA molecule is anchored to two beads or a bead and a surface and then stretched and analyzed, and DNA curtains, where many DNA molecules are anchored to a lipid bilayer and stretched using liquid flow (Collins *et al.*, 2014). For genomic analysis, DNA can be efficiently stretched on glass surfaces using molecular combing (Bensimon *et al.*, 1994; Neely *et al.*, 2011), allowing high-throughput analysis.

The computer industry has pushed a revolution to miniaturize components, such as transistors, resulting in the development of methods for efficient nanofabrication on length scales of tens of nanometers. The same methods have later been applied to a plethora of other disciplines where miniaturization is desirable, not the least in microfluidic and nanofluidic applications in the life sciences. Nanofluidic devices have many appealing features that make them useful for analyzing single long DNA molecules. Channels of nanoscale dimensions allow stretching of long DNA molecules to an extension close to their full contour length. Importantly, this can be done without anchoring any of the DNA ends, which for example allows analysis of DNA extracted from cells, circular DNA, and interactions occurring at DNA ends.

In this review we will first discuss the basic physics of nanoconfined DNA in detail. We will consider the early theories by de Gennes and Odijk, describing confined polymers, and how they have been gradually improved in order to fully cover the confinement regimes of importance in experiments. In the next section we will discuss how the nanofluidic devices can be fabricated and tailored for the project of interest, for example to obtain maximum stretching of the DNA, vary the degree of stretching, or monitor the response of the DNA upon addition of a solute in real time. Finally, we turn to the two main application areas of studying single DNA molecules in nanofluidic devices: optical DNA mapping (ODM) and DNA–protein interaction studies. For ODM we mainly focus on the technical aspects of the method. Recent years have presented a large increase in literature using ODM for genetic analysis, but these will only be briefly mentioned. For DNA–protein interactions, we will present several different examples that highlight the usefulness of nanofluidic channels for such studies and at the same time present the biological insight they have provided. [Figure 1](#) schematically illustrates the topics covered by this review.

## Theory

### Length scales characterizing DNA in free solution

The conformations of DNA are characterized by a cascade of length scales: the contour length  $L$ , representing the total length of the DNA backbone, the persistence length  $l_p$ , representing the characteristic length scale for bending that backbone under thermal energy, and the effective width  $w$ , representing the length scale for excluded volume interactions between distal segments of

the polymer. These fundamental length scales can be combined to produce a number of useful derived quantities, in particular the radius of gyration  $R_g$ , which provides a measure of the total size of the polymer, the thermal blob size (correlation length)  $l_b$ , which separates the highly correlated, short-range interactions between local segments of the polymer from the decorrelated, longer-range interactions, and the excluded volume  $v_{ex}$ . All of these length scales play a role in understanding the thermodynamics of DNA in confinement.

### Fundamental length scales

The smallest of the length scales characterizing the conformations of DNA is the width of the DNA backbone. While the steric dimension of the backbone is approximately 2 nm, electrostatic repulsion arising from the charged phosphate groups makes the DNA backbone appear thicker than would be expected, were the DNA a neutral polymer. The standard approach to treat the electrostatics is to consider an effective width  $w$  (Stigter, 1975, 1977), which is obtained from a mapping of the osmotic pressure produced by a suspension of charged cylinders of diameter  $d$  to that produced by neutral cylinders of ‘effective width’  $w$ . For the high ionic strength buffers sometimes used in experiments of confined DNA, for example 100 mM of monovalent salt, Stigter’s theory (Stigter, 1977) produces an effective width of approximately 5 nm. At lower ionic strength, the effective width is available from Stigter’s theory and numerical results have been reported, for example, by Hsieh *et al.* (2008) or Tree *et al.* (2013a). When making this mapping, the details of the electrostatic interactions are replaced by an equivalent neutral polymer model.

At the next level up is the DNA persistence length  $l_p$ , which reflects the decay of the correlations between the tangent vectors along the DNA backbone. A qualitative (but useful) way to think about the persistence length is that it characterizes the ability of the DNA to be bent by thermal energy. For high ionic strength buffers, the persistence length of DNA is approximately 50 nm, a frequently cited result obtained by Bustamante *et al.* using magnetic tweezers (Bustamante *et al.*, 1994). The persistence length is also affected by ionic strength, since the ions in solution screen the charges along the DNA backbone and thus affect its propensity to bend under thermal energy (Odijk, 1977; Skolnick and Fixman, 1977). Similar to the effective width, it is convenient to subsume the details of the electrostatic interactions into a persistence length that captures both the intrinsic contributions, arising from the steric interactions, and an electrostatic contribution. After the mapping is complete, we now have an equivalent neutral polymer model for the DNA that is thicker (due to the effective width) and stiffer (due to the electrostatic contribution to the persistence length) than would be expected based solely on the steric volume of its constituent atoms.

To account for electrostatic contributions to the persistence length, Dobrynin (2005) proposed a semi-empirical formula to correct for the ionic strength dependence, correcting an approximation in the classic Odijk–Skolnick–Fixman (OSF) theory by Odijk (1977) and Skolnick and Fixman (1977). Hsieh *et al.* (2008) showed that the Dobrynin model provides a superior description of DNA confined to a nanoslit when compared to the OSF theory. Subsequently, Chuang *et al.* (2017) extended Dobrynin’s result to further incorporate sequence effects. Their analysis of the stretching of human DNA in 45 nm nanochannels, when combined with Odijk’s theory for strong confinement (Odijk, 1983; Burkhardt *et al.*, 2010) and Dobrynin’s theory

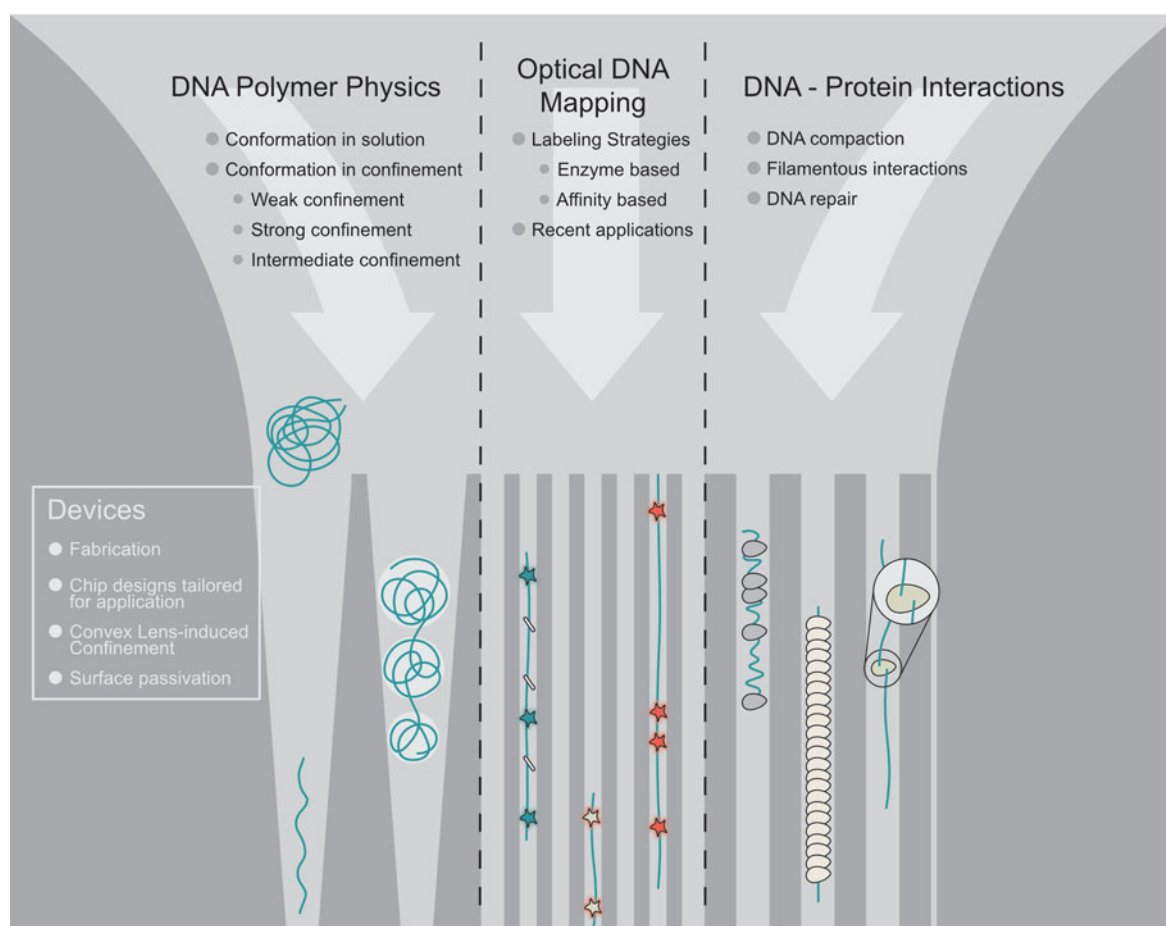


**Fig. 1.** Schematic overview of the topics covered by this review. In the first section a thorough introduction to the polymer physics of DNA is given, including a presentation of the length scales characterizing DNA conformation in solution and in different regimes of confinement. The following section is focused on the nanofluidic device and how the device design can be tailored for specific applications. Finally, two major application areas are reviewed: optical DNA mapping, describing how sequence information can be obtained from long DNA molecules stretched in nanofluidic channels, and DNA-protein interaction studies, showing examples of how nanofluidic channels can be utilized to investigate and understand the interaction between DNA and various types of proteins.

(Dobrynin, 2005), yielded the useful formula,

$$l_p \text{ [nm]} = (23 + 33\gamma + 26\gamma^2) + \frac{1.9195}{\sqrt{I[\text{M}]}} \quad (1)$$

where  $\gamma$  is the fraction of G-C base pairs. In the second term, which is the electrostatic contribution attributed to Dobrynin (2005),  $I$  is the ionic strength of the buffer. The details surrounding the role of electrostatics and counterion chemistry on the persistence length remain a subject of investigation (Brunet *et al.*, 2015; Trizac and Shen, 2016; Guilbaud *et al.*, 2019), and their impact on nanochannel DNA confinement is also complicated (Chuang *et al.*, 2019). These additional factors affect the quantitative agreement between theory and experiment.

At the longest length scale, at least for problems of interest to us here, is the DNA contour length  $L$ . At first glance, this appears to be a very straightforward quantity to compute; simply multiply the number of base pairs by the 0.34 nm/bp rise of B-DNA. However, fluorescence microscopy experiments typically require labeling of the DNA backbone with an intercalating dye, such as YOYO-1, that increases the extension of the DNA (Perkins *et al.*, 1995; Bakajin *et al.*, 1998; Randall and Doyle, 2005; Jeffet *et al.*, 2016; Lee *et al.*, 2018b). At full intercalation, the DNA contour length

can increase by circa 20–30% (Dorfman, 2010; Nyberg *et al.*, 2013). Kundukad *et al.* (2014) provide a concise review of different reports for DNA contour length increase upon YOYO-1 intercalation; we have found it convenient to assume that each bound dye molecule adds 0.51 nm to the DNA rise (Gupta *et al.*, 2018).

#### Derived length scales

While the trio of the contour length, persistence length, and effective width describe the length scales of the DNA chain, particular combinations of these parameters are often more useful for describing the configurations of a polymer. For a particularly lucid discussion of polymer conformations in general, consult the Perspectives article by Wang (2017). For the moment, we will focus on the relevant parameters for understanding DNA confinement, adopting typical length scales  $w = 5$  nm and  $l_p = 50$  nm for model calculations. We also further focus on the limit of chains where  $L \gg l_p$ , which are coils rather than rods (Hiemenz and Lodge, 2007). For  $\lambda$ -DNA (48.5 kbp), which is a commonly used model system, the stained contour length at full intercalation is close to 20  $\mu\text{m}$  (Tegenfeldt *et al.*, 2004), corresponding to 400 persistence lengths assuming no effect of the dye on the persistence length (Gunther *et al.*, 2010; Kundukad *et al.*, 2014; Dorfman, 2018).

The size of the coiled chain is characterized by either the end-to-end distance or the radius of gyration,  $R_g$ , of the polymer. While either metric is suitable for our purposes, we will focus here on the radius of gyration. For an ideal polymer, the radius of gyration is given by random walk statistics,

$$R_g^2 = \frac{Nb^2}{6}, \quad (2)$$

where  $N$  is the number of statistical segments and  $b$  is the statistical segment length (Hiemenz and Lodge, 2007); it follows that  $L = Nb$ . The exponent characterizing the scaling for the radius of gyration of an ideal chain is thus  $N^{1/2}$ . For a semiflexible chain like DNA, the correspondence between the random walk statistics and the Kratky and Porod (1949) result for the end-to-end distance of a long wormlike chain gives  $b = 2l_p$ .

When excluded volume is important, the chain obeys self-avoiding random walk statistics with a radius of gyration

$$R_g \cong L^{3/5} l_p^{1/5} w^{1/5}. \quad (3)$$

Comparing Eqs. (2) and (3), the exponent for the scaling of the polymer size changes from  $N^{1/2}$  for an ideal chain to  $N^\nu$  in the presence of excluded volume, where we have made the trivial conversion between contour length and degree of polymerization,  $L \sim N$ . The parameter  $\nu$  is known as the Flory exponent, and accounts for the additional swelling of the polymer coil caused by the excluded volume between distal segments. In Eq. (3), we have used the classical value of the Flory exponent  $\nu = 3/5$  to quantify the scaling for the chain size; the most accurate estimate of the scaling exponent by Clisby is  $\nu = 0.587597(7)$  (Clisby, 2010).

When is excluded volume important? To answer this question, we first need to understand the excluded volume interactions between different segments of the DNA. The cross-over is typically written in terms of an excluded volume parameter (Wang, 2017),

$$z = \left(\frac{3}{2\pi}\right)^{3/2} \left(\frac{\nu_{ex}}{b^3}\right) N^{1/2}. \quad (4)$$

The Onsager excluded volume,  $\nu_{ex}$ , between two cylindrical rods of width  $w$  and length  $l_p$  is approximately  $\nu_{ex} \cong l_p^2 w$ . To determine the length scale over which excluded volume matters, we set  $z \cong 1$ . The number of statistical segments required to satisfy this condition is then  $b^6/\nu_{ex}^2$ . Using Eq. (2), the thermal blob size,

$$l_b \cong \frac{b^4}{\nu_{ex}} \quad (5)$$

is defined as the size of a polymer chain where  $z \cong 1$ , which is conventionally taken as the point at which excluded volume becomes important. In the standard polymer physics interpretation (Wang, 2017), a polymer whose radius of gyration exceeds the thermal blob size is affected by excluded volume.

While these scaling arguments are useful for establishing the general phenomena, the neglect of various prefactors makes them less useful for modeling DNA in nanochannel experiments. Indeed, Tree *et al.* (2013a) pointed out that there are several equally plausible definitions of the thermal blob size and these definitions give remarkably different results for the onset of excluded volume for DNA, ranging from 16.8 to 166 kbp. These values span the range of typical DNA sizes used in experiments.

To be more quantitative, Tree *et al.* (2013a) instead computed the Flory exponent for DNA as a function of the number of base pairs in the relationship  $R_g \sim N^\nu$ , leveraging the renormalization group result from Chen and Noolandi (1992). Figure 2 shows that typical molecular size standards, such as  $\lambda$ -DNA, obey neither Eq. (2) nor Eq. (3). Rather, typical DNA sizes used in the experiments discussed here are in a very broad cross-over between ideal chain scaling and self-avoiding random walks.

In what follows, we will define the thermal blob size,

$$l_b \cong \frac{l_p^2}{w} \quad (6)$$

as this definition has proven to be very useful for defining the onset of the de Gennes regime for a confined polymer. For DNA in a high ionic strength buffer, this definition of the thermal blob size is approximately 500 nm, corresponding to approximately  $2.5 \mu\text{m}$  of DNA. This length scale will play an important role in defining the extent of confinement in what follows.

### Wall depletion length

When DNA is confined to a nanochannel, there is an additional length scale characterizing the DNA-wall interactions. Both the DNA and the walls are negatively charged and therefore repel one another. In the simplest model, one can capture this effect by introducing a depletion length  $\delta$  such that the effective channel size is  $D_{\text{eff}} = D - \delta$ . Several models have been proposed for the depletion length, including using the DNA effective width  $w$  (Wang *et al.*, 2011), a rigid-rod approximation (Reisner *et al.*, 2012), and a semiflexible chain model (Reisner *et al.*, 2012). Bhandari *et al.* (2018) measured this depletion length at different ionic strengths using a high-throughput genome mapping approach and found that their data were described by the simple phenomenological model  $\delta = 6.5 \lambda_D + 0.64$ , where  $\lambda_D$  is the Debye length of the buffer solution.

### Configuration of DNA in channel confinement

Having reviewed the relevant theory for the configurations of DNA in free solution, we now consider its configuration when

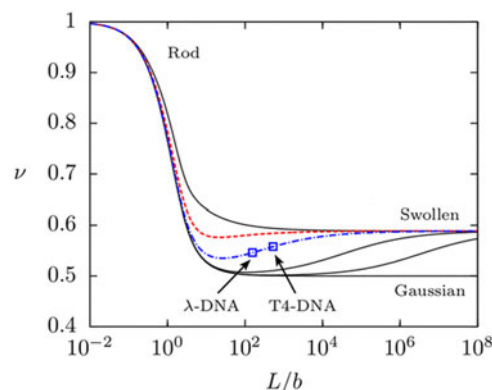


**Fig. 2.** Flory exponent  $\nu$  as a function of the number of statistical segments obtained from renormalization group calculations (Chen and Noolandi, 1992). The curves correspond to different values of  $w/b$ , where the upper (red) dashed line is a typical value for single-stranded DNA and the lower (blue) dashed line is a typical value for double-stranded DNA. The locations for  $\lambda$ -DNA (48.5 kb) and T4-DNA (166 kb) are denoted by boxes. The asymptotic limits of a rod, random walk (Gaussian chain), and self-avoiding random walk (swollen chain) are indicated. Reproduced with permission from (Tree *et al.*, 2013a), © 2013 American Chemical Society.

confined to a square nanochannel of size  $D$ . Much of the literature, in particular for genomics applications in nanochannels, describe the confined DNA as being stretched, and this nomenclature will be adopted for our review. However, this nomenclature is not quite correct, since ‘stretching’ a polymer implies that a force is applied to oppose the entropic elasticity, for example when using tweezers (Bustamante *et al.*, 1994). It is more precise to say that the DNA becomes ‘extended’ since it is compressed from its free solution radius of gyration by the walls, which causes the DNA to extend along the channel axis. There are subtle distinctions between compression and stretching (Dai and Doyle, 2013).

There are two key metrics to consider; the first is the size of the chain. While we could continue to describe the size of the chain by its radius of gyration in confinement (or the end-to-end distance), it is particularly convenient to use the mean span  $X$  of the confined DNA because this size can be directly measured by fluorescence microscopy. If we denote by  $x(s)$  the axial coordinate of the part of the DNA located at  $s \in [0, L]$ , the span of that configuration is defined as

$$X = \max x(s) - \min x(s). \tag{7}$$

It is also important to understand the variance about the mean span,

$$\sigma^2 = (X - \bar{X})^2, \tag{8}$$

which measures the effects of thermal fluctuations. Note that the mean span of a polymer in free solution is zero, since the random walk has, on average, no net displacement from the origin. (The radius of gyration is related to the variance in the chain size.) When a polymer is confined to a nanochannel, excluded volume effects and its stiffness force it to extend along the channel axis, producing a non-zero value of the mean span.

We focus here on the span of the confined molecule because it is experimentally accessible via fluorescence microscopy. For sufficiently long chains, the mean span and end-to-end distance converge to a single value because end effects make a negligible contribution (Muralidhar *et al.*, 2014b; Smithe *et al.*, 2015). However, the contour length at which these various metrics converge can be very long and depends on the channel size.

The different regimes of confinement are summarized by Fig. 3. We discuss each of these models in detail below.

*De Gennes regime (weak confinement)*

Daoud and De Gennes (1977) developed the classic treatment of the extension of weakly confined polymers. By weak confinement, we mean that the channel size is smaller than the radius of gyration (so that the DNA needs to extend along the channel axis), but larger than the thermal blob size in Eq. (6). The latter restriction implies that the subchain within a correlation length  $D$  is itself a self-avoiding walk that obeys Eq. (2). The contour length of the subchain, which is also referred to as a blob and indicated by the circle in Fig. 3, is given by  $L_{\text{blob}} \cong D^{5/3} l_p^{-1/3} w^{-1/3}$ . The number of blobs is  $N_{\text{blob}} = L/L_{\text{blob}}$  and the mean span of the chain is  $X \cong N_{\text{blob}} D$ . Putting these results together gives the de Gennes scaling for a confined polymer,

$$X \cong L \left( \frac{w l_p}{D^2} \right)^{1/3}. \tag{9}$$

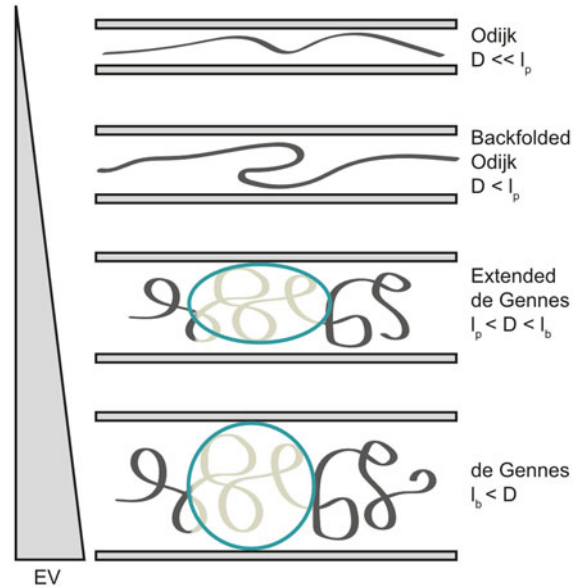


**Fig. 3.** Schematic illustration of the different regimes of confinement as the channel size  $D$  increases. The approximate boundaries of the channel size relative to the chain persistence length  $l_p$  and thermal blob size  $l_b$  are indicated. The circles, and highlighted part of the sketched polymer, indicate the anisotropic and isotropic blobs in the extended de Gennes regime and de Gennes regime, respectively. As the channel size increases, the excluded volume (EV) interactions between segments of DNA become stronger.

The variance in the chain size is  $\sigma^2 \cong N_{\text{blob}} D^2$ , which gives (Dai and Doyle, 2013)

$$\sigma^2 \cong L(Dw l_p)^{1/3}. \tag{10}$$

While these results are derived in the context of blob theory, equivalent results are obtained from a modified Flory theory (Jun *et al.*, 2008; Wang *et al.*, 2011). The prefactors for the scaling laws can be computed via simulations (see, e.g. Muralidhar *et al.*, 2014b), but they are expected to be  $O(1)$  quantities. For the purpose of understanding experimental data, the exact value of the prefactor is not particularly important.

*Odijk regime (strong confinement)*

Odijk (1983) considered the opposite case to Daoud and de Gennes, where the polymer is strongly confined in a channel that is much smaller than its persistence length. Here, rather than forming a series of blobs, Odijk showed that the DNA instead forms a chain of deflection segments of characteristic size  $\lambda \cong D^{2/3} l_p^{1/3}$ , which is known as the deflection length. In essence, the chain performs a persistent random walk due to its stiffness, but the collisions with the hard wall over distances corresponding to the deflection length lead to decorrelations between different segments of the chain.

In the absence of any hairpin turns, the extension of this chain of deflection segments is

$$\langle X \rangle = L \left[ 1 - 0.18274 \left( \frac{D}{l_p} \right)^{2/3} \right], \tag{11}$$

where the prefactor for a square channel was computed by Burkhardt *et al.* (2010) from an accelerated particle model.

These authors further computed the variance in the chain extension, arriving at

$$\sigma^2 = 0.00956 \frac{D^2}{l_p} L. \quad (12)$$

Corrections for rectangular channels (Burkhardt *et al.*, 2010) and circular channels (Yang *et al.*, 2007) are available, and slightly different results have been obtained from different calculations (Chen, 2016).

The statistics for strongly confined chains in the Odijk regime and weakly confined chains in the de Gennes regime are markedly different. In the de Gennes regime, the chain is only weakly perturbed from its coil shape and the dependence of the chain extension on channel size is strong. In contrast, the Odijk regime corresponds to almost completely extended chains, since the energetic cost to form a hairpin is extremely high (Odijk, 2006). The extension of the chain in the Odijk regime thus has a very weak dependence on the channel size. The increase in extension as the channel size decreases in the Odijk regime is driven by alignment of the deflection segments along the channel axis, which increases as the channel size decreases. This orientation effect is also the reason why the variance in the Odijk regime decreases with decreasing channel size; as the alignment fluctuations are suppressed, the fluctuations in the chain extension are also suppressed. The fluctuations in the chain extension also decrease with decreasing channel size in the de Gennes regime, albeit more weakly. The reason for the weaker decay in fluctuations is that these fluctuations are driven by the blobs, not by orientation of the chain with the channel axis.

#### Additional scaling regimes at intermediate confinement

While the de Gennes and Odijk regimes possess an aesthetic beauty as physical models, they are of little use in describing the extension of DNA in confinement. If we take a thermal blob size of 500 nm, then a conservative estimate of the start of the de Gennes regime is a channel that is several microns in size. However, in order to reach de Gennes statistics, the DNA in such a large channel needs to comprise several blobs (Muralidhar *et al.*, 2014b). If we use an aggressive set of bounds and set  $D = 1 \mu\text{m}$  and only one blob, we get a minimum contour length of  $L = 16 \mu\text{m}$ . In principle, we would like to be at least an order of magnitude away from this boundary, which would imply we need circa 500 kbp long DNA. While such long molecules have been used in some physics experiments (Tegenfeldt *et al.*, 2004; Freitag *et al.*, 2015) and are routinely used for genome mapping in nanochannels (Müller and Westerlund, 2017), most physical experiments use shorter DNA and/or narrower channels.

At the other end of the spectrum, the Odijk regime requires that the channel size be much smaller than the persistence length. For high ionic strengths, the requisite channel sizes are below the 20 nm lower bound for injecting DNA (Cao *et al.*, 2002b) and the smallest channels used for measuring DNA extension (Reisner *et al.*, 2005). It is possible to work with wider channels and remain in the Odijk regime by decreasing the ionic strength (Jo *et al.*, 2007; Kim *et al.*, 2011; Kounovsky-Shafer *et al.*, 2017; Lee *et al.*, 2018b), and Odijk's theory seems to be a good description there. However, one does need to be careful in interpreting the data because the electrostatic double-layers from the walls now occupy a substantial fraction of the channel cross-section, complicating the mapping from the polyelectrolyte problem to the

neutral polymer model embodied by Odijk's theory (Reisner *et al.*, 2012; Cheong *et al.*, 2017; Chuang *et al.*, 2019; Bhandari and Dorfman, 2020). From a fundamental perspective, the best way to probe the Odijk regime using biopolymers is to switch to stiffer molecules, such as actin (Noding and Koster, 2012) or RecA filaments (Frykholm *et al.*, 2014).

Using scaling theory, Odijk (2008) identified two additional regimes that should exist between what are now referred to as the classic de Gennes regime and the classic Odijk regime. As the channel size decreases below the thermal blob size ( $\sim 500$  nm) but remains above the statistical segment length ( $\sim 100$  nm), the blobs become ellipsoidal, as indicated in Fig. 3, and their statistics are marginal, i.e. the excluded volume corresponds to  $z \cong 1$ . This regime of confinement is often referred to as the 'extended de Gennes' regime (Wang *et al.*, 2011) because the scaling for the extension given by Eq. (9) 'extends' to even smaller channel sizes. However, the variance of the chain extension is markedly different in the extended de Gennes regime,

$$\sigma^2 = Ll_p. \quad (13)$$

The latter result, which can be derived using either blob theory (Dai and Doyle, 2013) or modified Flory theory (Wang *et al.*, 2011), is remarkable – the fluctuations of the confined, real chain are equal to those of an unconfined, ideal chain of the same contour length. The independence of the variance from the channel size was a key to providing affirmative proof for the existence of the extended de Gennes regime in simulations (Dai and Doyle, 2013) and experiments (Gupta *et al.*, 2015; Iarko *et al.*, 2015). However, the best theoretical evidence in support of the extended de Gennes regime lies in the excess free energy of confinement (Dai *et al.*, 2014), which put to rest a lingering discussion over the existence (or lack thereof) of this regime (Tree *et al.*, 2013b), but this small change in free energy is not straightforward to measure via experiments.

The extended de Gennes regime has a strong connection with the theory of marginal solutions of semiflexible polyelectrolytes (Schaefer *et al.*, 1980; Dai *et al.*, 2014; Wang, 2017). Werner and Mehlig (2014) also recognized a connection between the statistics of the extended de Gennes regime and weakly self-avoiding random walks. Leveraging exact results for weakly self-avoiding walks in the mathematical literature, they were able to provide exact prefactors for both the extension and variance in the extended de Gennes regime. Data from subsequent experiments (Gupta *et al.*, 2015; Iarko *et al.*, 2015) were in good but not quantitative agreement with the theoretical predictions. Subsequently, Schotzinger *et al.* (2020) provided conclusive evidence for the extension scaling in the extended de Gennes regime, explaining previous disagreements between theory and experiment as the result of inadequate characterization of the channel cross-section that were circumvented in their experiments by using a focused-ion beam approach to channel fabrication (Menard and Ramsey, 2013).

When the channel size is below the statistical segment length ( $\sim 100$  nm), Odijk (2008) predicted a cross-over from blob statistics to deflection segments. However, unless the channel size is much smaller than the persistence length, the chain can still form the hairpins indicated in Fig. 3 because the energy of formation is not particularly high (Polson, 2018), a phenomenon identified via simulations by Cifra and Bleha (2012) and Dai *et al.* (2012). Odijk (2006) called the length scale for forming a hairpin the global persistence length  $g$ .

The presence of hairpins within the chain invalidates the results in Eqs. (11) and (12). When the chain can form hairpins, Odijk showed that its statistics are described by a different scaling variable (Odijk, 2008; Muralidhar *et al.*, 2014a)

$$\xi = \frac{g^w}{D^{5/3}l_p^{1/3}} \tag{14}$$

that measures the total excluded volume created by a hairpin to the spatial volume  $gD^2$  occupied by that hairpin. Using a Flory argument, Odijk (2008) then derived the scaling

$$\langle X \rangle \cong L\xi^{1/3} \tag{15}$$

for the chain extension when  $L \gg g$ , i.e. when the chain can form many hairpin folds. The concomitant variance in the chain extension is

$$\sigma^2 \cong gL. \tag{16}$$

Comparing Eqs. (16) and (13) shows that the variance in the extended de Gennes regime and backfolded Odijk regimes is of the same form, but the persistence length of the polymer needs to be replaced by the global persistence length to describe the backfolded Odijk regime.

Muralidhar *et al.* (Muralidhar *et al.*, 2014a, 2016; Muralidhar and Dorfman, 2016) undertook systematic studies of the backfolded Odijk regime via simulations. In addition to providing a pedagogical introduction (Muralidhar *et al.*, 2014a) to Odijk’s scaling theory (Odijk, 2008), they confirmed all predictions of Odijk’s theory for square, rectangular, and circular channels. Importantly, the simulation work by Muralidhar *et al.* (2014a) identified a shortcoming in Odijk’s theory for the global persistence length (Odijk, 2006), which plays a key role in the overall theory. The disagreement between Odijk (2006) and Muralidhar *et al.* (2014a) was resolved by Chen (2017), who provided a complete correction to Odijk’s theory.

Owing to the very large increase in the global persistence length as the channel size decreases (Odijk, 2006), Eq. (16) predicts an equally large increase in the fluctuations of the extension in this regime. These large fluctuations were not realized in experiments with DNA because the DNA was too short to form the large hairpins predicted by Odijk’s theory (Su *et al.*, 2011). Indeed, experiments to probe the backfolded Odijk regime using DNA are infeasible (Muralidhar *et al.*, 2014a).

### Telegraph model for intermediate confinement

The schematic illustration of different regimes in Fig. 3 is not entirely correct; the boundaries are listed as inequalities but, strictly speaking, correspond to strong inequalities. The relatively good agreement between theory and experiment for the extended de Gennes regime (Gupta *et al.*, 2015; Iarko *et al.*, 2015; Schotzinger *et al.*, 2020) suggests that those inequalities are not especially strong. However, there are no experimental data to support the existence of a backfolded Odijk regime for DNA. While it is possible to probe the Odijk excluded volume by a non-equilibrium measurement (Krog *et al.*, 2018; Reifengerger *et al.*, 2018), we seem to be again stuck in a situation where there is an elegant scaling theory that says little about the problem of DNA confinement.

Werner *et al.* (2017) recognized that the exact theory for the extended de Gennes regime (Werner and Mehlig, 2014) applies

for all confinements below the thermal blob size but outside the Odijk regime. In other words, there is no reason to distinguish between the deflection segments in the backfolded Odijk regime and the blobs in the extended de Gennes regime. Rather, the key to understanding intermediate confinement is to recognize the weakness of excluded volume interactions for  $D \ll l_p^2/w$ . While the chain can fold back on itself in these smaller channels, the long distance along the contour length causes the chain to ‘forget’ the previous configurations. As a result, the excluded volume interactions can be treated in a mean-field sense (Chen, 2018).

Thus, instead of relying on the extended de Gennes or backfolded Odijk models, the DNA statistics for  $D \ll l_p^2/w$  can be described by the weakly-correlated telegraph model. The telegraph model describes a random walk that moves at a fixed velocity with the random changes in direction indicated in Fig. 4. In the weakly correlated telegraph model, there is a small energy penalty  $\varepsilon$  when the chain revisits a lattice site. This one-dimensional model is easily simulated to produce predictions for  $X$  and  $\sigma^2$ . Importantly, the telegraph model predicts that these parameters should collapse as a function of the scaling parameter

$$\alpha = \frac{\varepsilon g}{a} \tag{17}$$

where  $a$  quantifies the average alignment of the chain backbone with the channel axis. Remarkably, the limits of large  $\alpha$  (narrow channels) and small  $\alpha$  (wide channels), respectively, correspond to the parameter  $\xi$  for the backfolded Odijk regime in Eq. (14) and the scaling variable ( $wl_p/D^2$ ) in the extended de Gennes regime. As a result, the limits of the telegraph model are the backfolded Odijk and extended de Gennes regime (Werner *et al.*, 2017).

In addition to proposing the new scaling variable in Eq. (17), Werner *et al.* (2017) showed how the confined polymer problem maps to the correlated telegraph model. Explicitly, the various quantities appearing in the telegraph model can be computed from the statistics of an ideal semiflexible chain, i.e. when the only excluded volume interactions are between the polymer and the wall, and then the telegraph model provides a way to combine those statistics to predict the behavior of a real polymer. Figure 5 shows that the resulting predictions of the telegraph model are in almost exact agreement with three-dimensional simulation data for a confined wormlike chain (Werner *et al.*, 2017). The only disagreement between theory and simulation arises deep into the backfolded Odijk regime at large  $\alpha$ . Here, where hairpin turns are rare, the dominant contribution to the variance becomes the fluctuations in the alignment of the segments with the channel walls, which are not included in the telegraph model. Simply adding the variance of the telegraph model to the result in Eq. (12)

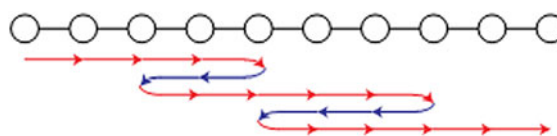
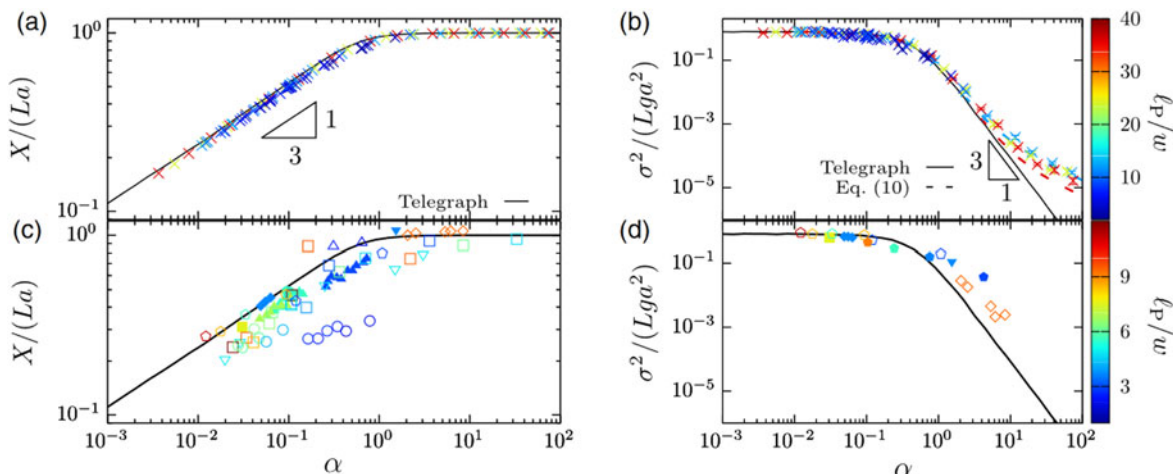


Fig. 4. Schematic illustration of the weakly correlated telegraph model (Werner *et al.*, 2017). The chain is replaced by a particle that moves at a constant velocity between lattice sites with random changes in direction. When a lattice site is revisited, there is an energy penalty.



**Fig. 5.** The telegraph model compared to simulations (a, b) and experiments (c, d), respectively. The dashed lines in (b) (referring to Eq. (10) in the original paper) is the sum of the variance predicted by the telegraph model and alignment fluctuations from Odijk's theory (Burkhardt *et al.*, 2010). The pertinent scaling laws are described by Werner *et al.*, (2017). Experimental data:  $\nabla$  (Reisner *et al.*, 2005),  $\square$  (Reisner *et al.*, 2007),  $\blacksquare$  (Thamdrup *et al.*, 2008),  $\circ$  (Zhang *et al.*, 2008),  $\bullet$  (Utiko *et al.*, 2011),  $\triangle$  (Kim *et al.*, 2011),  $\blacktriangle$  (Werner *et al.*, 2012),  $\blacktriangledown$  (Gupta *et al.*, 2014),  $\diamond$  (Reinhart *et al.*, 2015),  $\blacklozenge$  (Gupta *et al.*, 2015),  $\circ$  (larko *et al.*, 2015), and  $\bullet$  (Alizadehheidari *et al.*, 2015). Reproduced from Werner *et al.* (2017), © Werner *et al.* (2017) under Creative Commons CC BY 4.0.

for these alignment fluctuations restores the agreement between the theory and simulation. The collapse of the experimental data to the theory in Fig. 5 is also satisfying, especially in light of the possible sources of systematic errors that have been identified in the context of experimental work (Nyberg *et al.*, 2013; Gupta *et al.*, 2015; Iarko *et al.*, 2015; Schotzinger *et al.*, 2020).

Chen (2018) arrived at a similar scaling result to Eq. (17) using the self-consistent field theory solution for the wormlike chain propagator. Chen's theoretical approach is more robust and allows considering polymers that are much stiffer than DNA and inaccessible by the simulations needed to compute the parameters appearing in the telegraph model.

The telegraph model can also be solved exactly (Odman *et al.*, 2018) in the limit of relevance to genome mapping, where the channel cross-section is close to the DNA persistence length, providing a formula for predicting not only the mean span and its variance, but also the distribution for the chain extension. Simulations of semiflexible polymers by Bhandari and Dorfman (2019), including situations that mimic DNA-based experiments, showed that the asymptotic solution of Odman *et al.* (2018) is in quantitative agreement with simulations. Experimental data for the DNA extension distribution obtained in genome mapping experiments (Reinhart *et al.*, 2015; Sheats *et al.*, 2015), however, tend to exhibit increasingly worse agreement with the asymptotic solution to the telegraph model as the channel size decreases. This behavior is in contrast to the expectations of the theory of Odman *et al.* (2018), that infer improved agreement as the channel size decreases. Subsequent experiments and theory by Chuang *et al.* (2019) suggest that this disagreement is due to the simplified approach to DNA-wall electrostatic interactions used to model DNA, not an inherent problem in the telegraph model itself.

#### Effect of channel geometry

The discussion thus far has focused primarily on square nanochannels of width  $D$ . From a theoretical perspective, there are only minor differences between a square channel and a circular channel of diameter  $D$  that arise from the entropic depletion of the DNA from the corners of the square channel (Odijk, 2006).

While simple to analyze from a theoretical perspective, these geometries are challenging to fabricate in practice. The most commonly encountered situation is rectangular nanochannels with a width  $D_1$  and a height  $D_2$ .

The first question to address is whether a rectangular cross-section is actually a nanochannel in the sense that we have discussed so far, or whether it is a slit. To answer this question, let us assume that  $D_1 > D_2$ , which is the easier case to fabricate, and recall what would happen in the case  $D_1 \rightarrow \infty$ . This situation corresponds to a nanoslit of height  $D_2$ . Daoud and De Gennes (1977) used scaling theory to demonstrate that the in-plane radius of gyration of a polymer confined to a slit consists of a two-dimensional, self-avoiding random walk of blobs. For a semiflexible polymer, Eq. (3) for a polymer in free solution becomes (Hsieh *et al.*, 2008)

$$R_{\text{slit}}^2 \sim L^{3/2} \left( \frac{l_p w}{D_2} \right)^{1/2} \quad (18)$$

when that polymer is confined to a slit. Provided that  $R_{\text{slit}} \gg D_2$ , then the system is a nanochannel because the DNA configuration will be influenced by the presence of the side wall. The latter inequality thus defines the cross-over between a nanoslit and a nanochannel.

Once we have confirmed that the system indeed corresponds to a nanochannel, we need to understand how the results for confinement discussed earlier are affected by the aspect ratio. To a first approximation, the theories for DNA confinement emerge from the random walk statistics of the confined chain (Chen, 2016). In the random walk statistics, the diffusion in different directions is decoupled. As a result, one can define the equivalent square channel size as  $D^2 = D_1 D_2$ . For aspect ratios that are not too far from unity, this approximation is sufficient. However, as the aspect ratio grows, additional complications arise because the way in which the confinement causes the DNA to extend along the channel axis depends on the channel size. This effect becomes particularly important for funnel-shaped nanochannels (Persson *et al.*, 2009). If the length scales  $D_1$  and  $D_2$  correspond



to different regimes of confinement, a ‘regime mixing’ effect occurs that complicates the analysis (Gupta *et al.*, 2014). It is possible to construct scaling theories that account for the regime mixing through the use of superblobs (Werner and Mehlig, 2015). However, the resulting theory now requires satisfying two strong inequalities, one for each of the channel dimensions, a situation that is unlikely to be realized in experiments. For rectangular channels, the most powerful approach to understanding the chain statistics is simulation (Gupta *et al.*, 2014; Muralidhar *et al.*, 2016).

In addition to rectangular channels, there is also a small body of literature on simulations of DNA confinement in triangular nanochannels (Manneschi *et al.*, 2013; Reinhart *et al.*, 2013; Han *et al.*, 2016), which are also relatively easy to fabricate by anisotropic etching of silicon. The entropic depletion effects of acute corners can be very significant, and the collapse of the extension data onto a universal curve is not straightforward (Reinhart *et al.*, 2013). Ultimately, triangular nanochannels have found interesting applications as collapsible systems for strongly extending DNA (Huh *et al.*, 2007) and chromatin (Matsuoka *et al.*, 2012) rather than as a system for fundamental studies.

### Effects of crowding agents

The physics of DNA extension in nanochannels changes in the presence of crowding agents, a phenomenon that has been explored experimentally (Zhang *et al.*, 2009, 2012; Jones *et al.*, 2011; Feng *et al.*, 2019; Scott *et al.*, 2019) and by simulation (Jones *et al.*, 2011; Liao *et al.*, 2015; Jeon *et al.*, 2016; Chen *et al.*, 2021). A particularly notable effect of crowding is the impact of confinement on the concentration required to compact the DNA by depletion effects induced on the DNA by the crowders. In experiments in the extended de Gennes regime, compaction was only observed in the nanochannels, not in the loading microchannels (Zhang *et al.*, 2009, 2012), illustrating the profound effect of the channel confinement on compaction. The effect of crowders is also sensitive to the chemistry of the compacting agent. For dextran, a model system for studying DNA compaction, the DNA initially extends at low concentrations of dextran but then compacts (Fig. 6) (Zhang *et al.*, 2009). In contrast, addition of bovine serum albumin (BSA) or hemoglobin to DNA in a nanochannel only produces compaction, with no

initial stage of extension (Zhang *et al.*, 2012). The addition of poly(ethylene glycol) at concentrations that do not induce compaction is even more complicated, with an extension behavior that cannot be captured by the scaling theories for DNA extension described above (Feng *et al.*, 2019).

When the crowding agent is provided at over-threshold volume fractions, compaction proceeds in two stages: a fast stage (circa 10 s) where the DNA extension in the channel is dramatically reduced, followed by a longer relaxation of several minutes where the DNA presumably reorganizes itself into an ordered structure (Zhang *et al.*, 2009). The reorganization and compaction of the blobs is a function of channel size. No compaction is observed for very small (60 nm × 100 nm) channels that are in the backfolded Odijk regime (Zhang *et al.*, 2012), possibly because there are no blobs and bending of the DNA is very unfavorable. The process of compaction changes qualitatively for slit-like confinement because there is room to reorganize the blobs in two unconfined dimensions (Jones *et al.*, 2011). As a result, for dextran crowding, there is a gradual transition from the apex of the extension induced by low dextran concentrations to the collapsed form at higher dextran concentrations (Jones *et al.*, 2011).

Simulations have explored the compaction process in the context of minimal models that are capable of producing the entropic depletion forces, qualitatively capturing the compaction process (Jones *et al.*, 2011), allowing for exploration of the relative effects of polymer–polymer and polymer–wall interactions induced by the depletion effects (Liao *et al.*, 2015), and providing insights that have enabled developing scaling-level models for the effect of crowders through an effective solvent picture (Jeon *et al.*, 2016). One of the most intriguing results emerging from simulations is the proposition that crowders could push the DNA toward the corners of the channel, thereby effectively increasing the confinement (Chen *et al.*, 2021). The latter prediction has not yet been explored experimentally.

### Outstanding challenges

While the problem of a confined linear DNA molecule has been largely resolved, two significant outstanding challenges remain in the modeling of nanochannel-confined DNA. The first problem emerges when the size of the electric double layer becomes commensurate with the size of the channel, as discussed already in

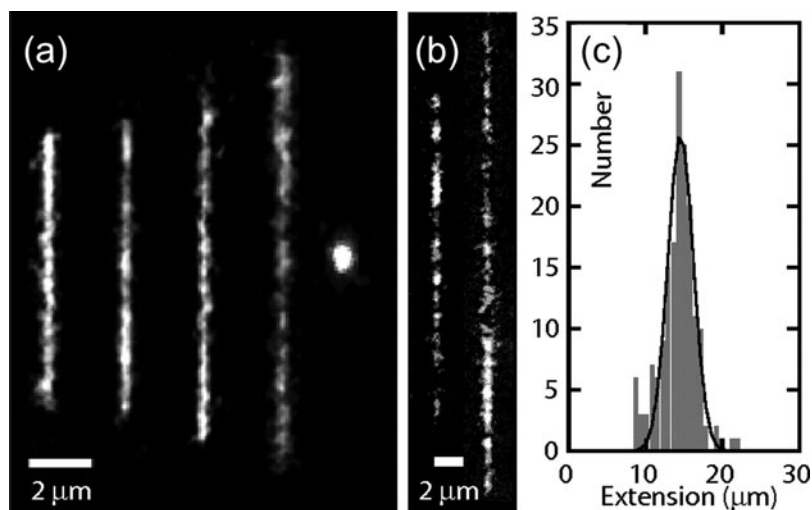


**Fig. 6.** (a) Single T4-DNA molecules, in 10 mM Tris buffer, confined to nanochannels ( $300 \times 300 \text{ nm}^2$ ) and crowded by dextran in increasing volume fractions ( $0$ ,  $4.2 \times 10^{-4}$ ,  $4.2 \times 10^{-3}$ ,  $4.2 \times 10^{-2}$ , and  $6.3 \times 10^{-2}$ ) from left to right. (b) As in (a), but in 1 mM Tris buffer,  $150 \times 300 \text{ nm}^2$  channels and dextran volume fractions  $4.2 \times 10^{-4}$  (left) and  $4.2 \times 10^{-2}$  (right). (c) Extension distribution for T4-DNA confined to  $300 \times 300 \text{ nm}^2$  channels, in 10 mM Tris buffer and a volume fraction of  $4.2 \times 10^{-2}$  of dextran ( $n=170$ ). Reproduced from (Zhang *et al.*, 2009), © (Zhang *et al.*, 2009).

section ‘Additional scaling regimes at intermediate confinement’. The second challenge is describing the configurations and dynamics of knotted DNA molecules (Micheletti, 2022). In the latter context, significant progress has been achieved by coarse-grained simulations (Micheletti and Orlandini, 2012, 2014; Orlandini and Micheletti, 2013; Suma *et al.*, 2015; Dai and Doyle, 2018; Polson and Hastie, 2020), at least for relatively small molecules. Experimental data have also started to emerge on knotted DNA in nanochannels (Metzler *et al.*, 2006; Amin *et al.*, 2018; Ma and Dorfman, 2020, 2021a, 2021b), enabled by the ‘knot factory’ platform (Amin *et al.*, 2018) that allows knots to be created at high enough frequency for studies at the single-molecule level. A key challenge in connecting these experimental data to simulations is the unknown and presumably high complexity of the knots created in these experiments when compared to the simpler knots used in simulations (Ma and Dorfman, 2020).

## Devices

Advances in fabrication of nanofluidic structures as well as design of devices for DNA applications make up important contributions to the progress of this research field. The fabrication and use of nanochannels for DNA studies at the single molecule level started in early 2000s (Cao *et al.*, 2002b; Tegenfeldt *et al.*, 2004). Since then, different materials and fabrication techniques have been explored (Duan *et al.*, 2013). In the following sections we will present commonly used fabrication processes in brief, as well as how channel and chip designs have developed in line with the expansion of the field, and we will give examples of designs tailored for different applications.

## Fabrication processes

The most reliable and documented method for nanochannel fabrication is the use of standard semiconductor device fabrication processes on silicon (Riehn *et al.*, 2005; Lam *et al.*, 2012) or fused silica (Tegenfeldt *et al.*, 2004; Reisner *et al.*, 2010; Freitag *et al.*, 2015) substrates in a cleanroom environment. A fresh silicon wafer with a 1–2  $\mu\text{m}$  thick thermal oxide layer (based on the depth of the micro- and nanofluidic channels) or a fused silica substrate is preferred. Typically, a 4- or 6-inch wafer is used, designed to contain an array of micro- and nanofluidic systems that subsequently can be diced to yield tens of devices from a single wafer.

The process of fabricating nanofluidic devices for DNA studies can be briefly described in the following steps: (1) Photolithography and reactive ion etching (RIE) of alignment marks that are used to align the micro- and nanofluidic features in the next steps. (2) Electron-beam lithography and RIE of the nanochannels. Focused ion-beam milling (Wang *et al.*, 2005; Menard and Ramsey, 2013), and nanoimprint lithography (Guo *et al.*, 2004) are well-established alternate methods that can be used to fabricate the nanochannels. (3) Photolithography and RIE of microchannels connecting the nanochannels. The design can be simply two straight microchannels connecting both nanochannel ends, where one microchannel serves as the inlet and the other as the outlet. Alternately, two U-shaped microchannels connecting the two ends of the nanochannels can be used to provide control in driving DNA into the nanochannels and minimize fouling. (4) Photolithography and deep reactive-ion etching of loading holes. Powder or sand blasting is a suitable alternate process for fused silica substrates to obtain loading holes. The loading holes are used for adding the sample liquid containing DNA to

the device, the DNA can then be driven into the microchannels and subsequently into the nanochannels using pressure-driven flow or electrophoresis. (5) High-temperature bonding of a glass wafer to the silicon or fused silica wafer to create the micro-nanofluidic confinement. Anodic bonding (Kutchoukov *et al.*, 2003; Abad *et al.*, 2011) and polymer fusion bonding involving a thin polymer intermediate layer (Gu *et al.*, 2007; Lesser-Rojas *et al.*, 2014) are alternate bonding techniques. All the fabrication steps discussed above are shown schematically in Fig. 7.

Fabrication of nanofluidic structures for DNA applications on silicon and fused silica wafers using traditional semiconductor fabrication processes is discussed in more detail in (Westerlund *et al.*, 2018). Further details on tools, chemicals, photoresists, and etching processes used for fabrication of nanofluidic devices on silicon wafers can be found in (Öz *et al.*, 2019; Kang *et al.*, 2022).

## Alternative fabrication

For many of the applications foreseen for nanofluidic devices, in particular in diagnostics, disposable chips produced at low cost are desirable. Several different strategies have been proposed for making chips using less demanding techniques and at higher throughput, compared to the traditionally used state-of-the-art nanofabrication processes. Nanofluidic chips for DNA analysis based on thermoplastic polymers can be fabricated by injection molding (Utko *et al.*, 2011) or nanoimprinting (Wu *et al.*, 2011; Uba *et al.*, 2015; Esmek *et al.*, 2019). Devices replicated in PDMS (van Kan *et al.*, 2012) from a nanofabricated master is another approach to increase fabrication throughput and decrease cost. Park *et al.* (2018) reported how near-field electrospinning can be used to create nanofluidic channels with a circular cross-section in PDMS, suitable for biological applications.

## Chip designs

### Tapered channels

By varying the channel dimensions along the channel length, it is possible to study the same individual, single DNA molecule at different degrees of confinement (Fig. 8a, b). In analogy to force spectroscopy, Persson *et al.* coined the concept confinement spectroscopy for probing single DNA molecules in tapered nanochannels (Persson *et al.*, 2009). Similar funnel-shaped channels were used by Frykholm *et al.* (2014) and Fornander *et al.* (2016), when studying the nucleoprotein filaments formed by RecA and Rad51, respectively, on DNA. Channels where the width is varied in discrete steps, rather than continuously tapered, have also been used, for example by Werner *et al.* (2018) and Gupta *et al.* (2015). The advantage of using discrete steps is that the DNA is not subjected to an entropic force that pushes it toward the larger end of the funnel, allowing equilibrium measurements to be performed at the cost of only doing so at a discrete number of channel dimensions.

### Devices for dynamic studies

The nanochannel device can be designed to add functionalities to it, such as the possibility to change the local environment around the DNA molecule under study, i.e. exchange buffers or add reagents to it. Such a set-up enables studies of, for example, DNA–protein interactions in real time.

A chip design presented by Zhang *et al.* features two arrays of parallel nanochannels in a perpendicular configuration (Zhang *et al.*, 2013b) (Fig. 8c). DNA is introduced into the device via

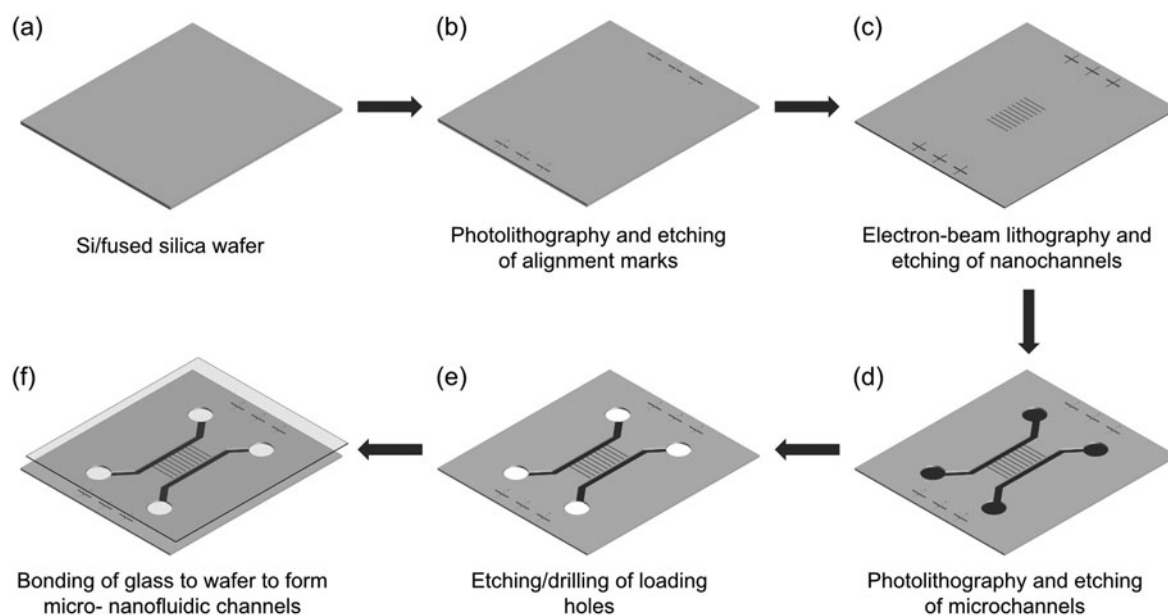


**Fig. 7.** Schematic illustration of the fabrication of a micro- and nanofluidic device, using traditional semiconductor fabrication processes. (a) Clean silicon or fused silica wafer used as a substrate. (b) Photolithography and reactive ion etching (RIE) of marks to help alignment of micro- and nanostructures. (c) Electron-beam lithography (EBL) followed by RIE to obtain nanochannels. (d) Microchannels aligned to the nanochannels, obtained using photolithography and RIE. (e) Formation of loading holes to enable sample loading. (f) Bonding of a glass slide to the silicon/fused silica wafer with fabricated features to obtain micro/nanoconfinement.

electrophoresis through the array of wider ( $250 \times 200 \text{ nm}^2$ ) nanochannels, whereas buffer can be exchanged via diffusion through the intersecting array of narrower ( $150 \times 200 \text{ nm}^2$ ) nanochannels in the perpendicular direction. As a proof of principle, compaction of T4-DNA upon addition of protamine and unpacking of pre-compacted T4-DNA by increasing salt concentration

were investigated, demonstrating the functionality of the device (Fig. 9a). Subsequently, the same device was used to study the interaction of the bacterial protein H-NS with DNA (Zhang *et al.*, 2013a).

Öz *et al.* (2019) designed a device enabling active exchange of the local environment within the nanofluidic channel (Fig. 8d).

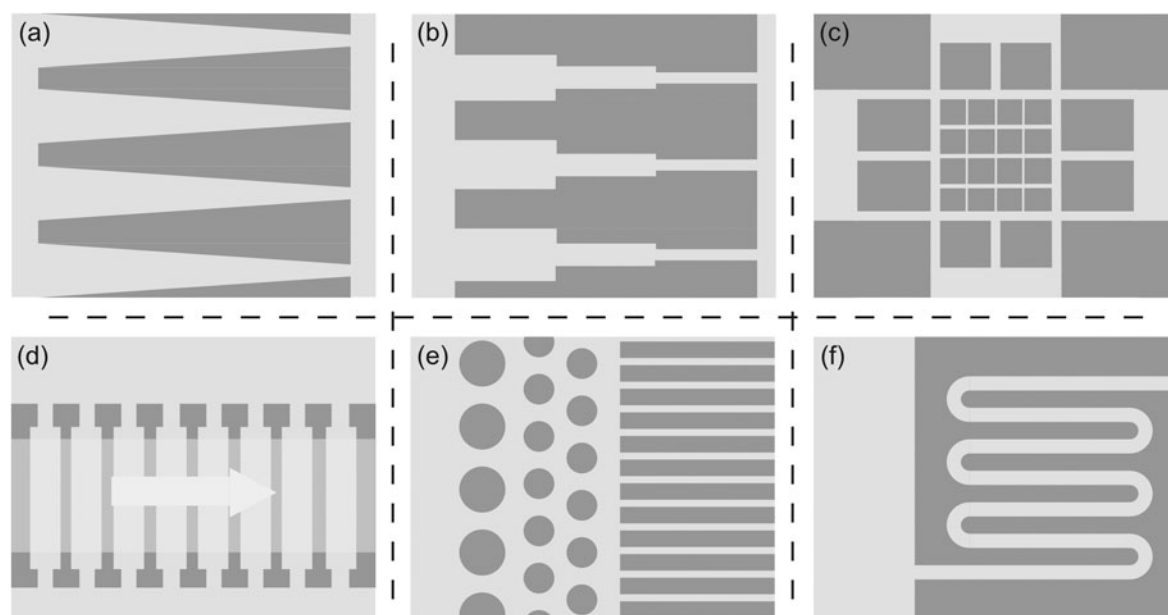


**Fig. 8.** Schematic illustration of chip designs tailored for different applications. (a–b) Varying channel dimensions, in a tapered or stepwise fashion, along the channel length enables studying the same individual, single DNA molecule at different degrees of confinement. (c) A chip design with perpendicular channel arrays enables diffusion driven buffer exchange. (d) Aligning a shallow slit on top of and orthogonal to reaction chambers, flanked by nanofluidic channels, enables active buffer exchange in the local environment of entrapped single DNA molecules. (e) Physical barriers that gradually increase the confinement can provide pre-stretching of DNA and reduce the thermodynamic cost of entering genomic sized DNA into nanochannels. (f) A meandering nanochannel design enables visualization of ultralong DNA molecules in a single field of view. The sketches are not drawn to scale.

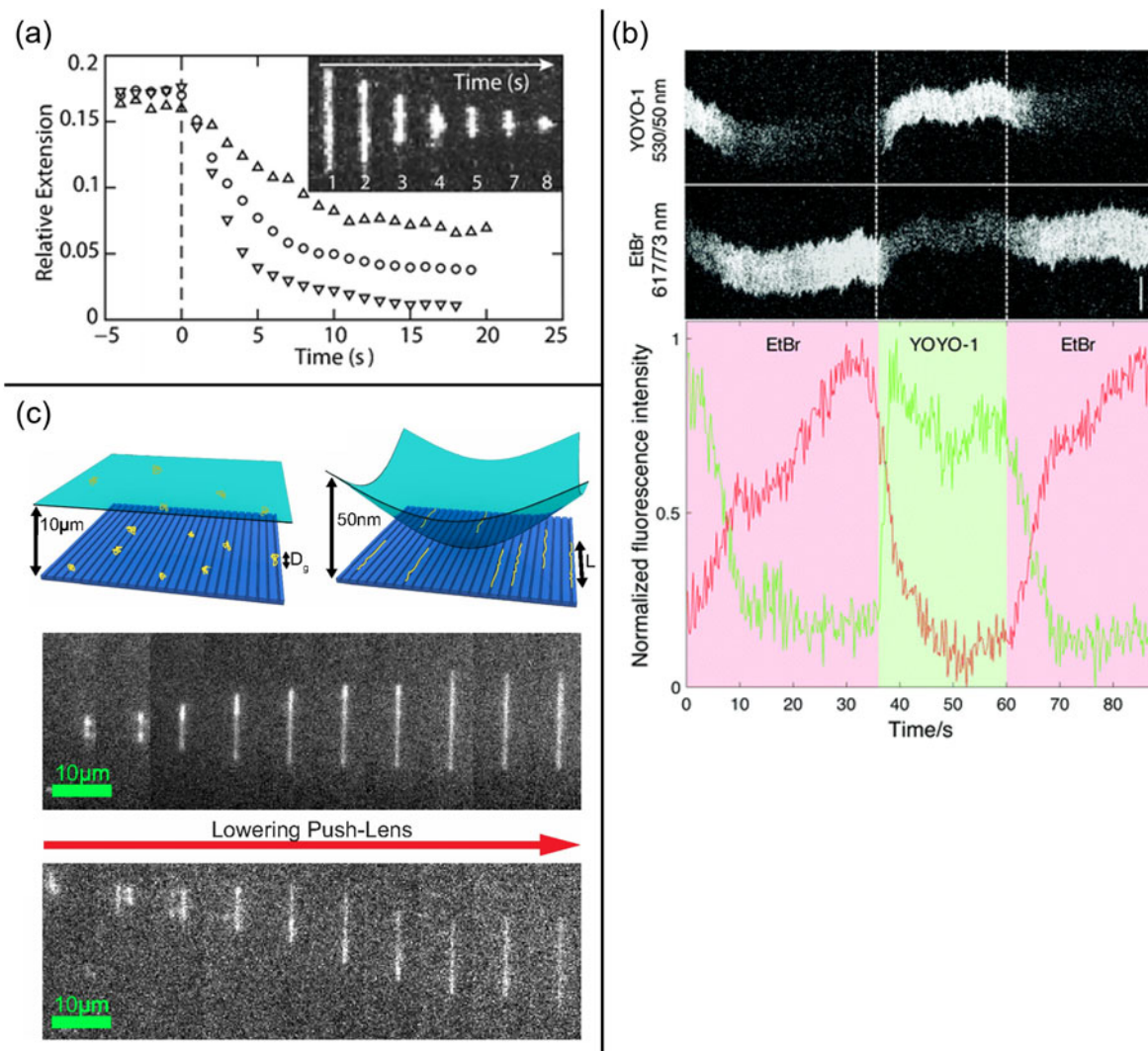


**Fig. 9.** (a) A nanofluidic device featuring two arrays of nanochannels oriented in a perpendicular configuration enables insertion of biomolecules through the channels in one direction and diffusion-driven buffer exchange through the intersecting, narrower, channels. The functionality was demonstrated by compaction of T4-DNA upon exposure to protamine (1 ( $\Delta$ ), 3 ( $\circ$ ) and 5 ( $\nabla$ )  $\mu\text{M}$ , respectively; inset shows fluorescence images of T4-DNA upon exposure to 5  $\mu\text{M}$  protamine). Reproduced with permission from Zhang *et al.* (2013b), © 2013 The Royal Society of Chemistry. (b) Demonstration of active exchange of the local environment in a nanofluidic reaction chamber by sequential addition of EtBr and SDS to YOYO-1 stained  $\lambda$ -DNA. Kymographs showing emission from YOYO-1 (top) and EtBr (center), respectively, and corresponding fluorescence intensity profiles (bottom) for YOYO-1 (green) and EtBr (red). Scale bar corresponds to 5  $\mu\text{m}$ . Reproduced from Öz *et al.* (2019), © Öz *et al.* (2019) under Creative Commons CC BY-NC 3.0. (c) Schematic illustration of the CLiC principle (top): DNA molecules in the solution are initially unconfined, as the height of the chamber is of microscale dimensions (left). Upon lowering the push-lens the chamber height is reduced to nanoscale dimensions and the DNA molecules are aligned to the nanochannels by confinement (right). Two series of fluorescence images showing the extension of  $\lambda$ -DNA as confinement increases while the push-lens is lowered. Center panel: channel width 27 nm and time between frames 364 ms; bottom panel: channel width 50 nm and time between frames 910 ms. Reproduced from (Berard *et al.*, 2014), © (Berard *et al.*, 2014).

The design includes an array of nanochannels ( $100 \times 100 \text{ nm}^2$ ), with a central stretch of slightly larger dimensions ( $300 \times 130 \text{ nm}^2$ ), creating an entropically controlled reaction chamber where single DNA molecules can be confined and stretched. Across the reaction chambers, on top of the array and in an orthogonal fashion, runs a shallow nano-slit ( $30 \mu\text{m} \times 30 \text{ nm}$ ), through which analytes actively can be introduced via pressure-driven flow to exchange the local buffer environment of the entrapped DNA molecule. The authors demonstrated the functionality of the device by a series of experiments, where analytes, such as SDS, spermidine, ethidium bromide and DNase I, were added to confined DNA molecules and the resulting response could be monitored *in situ* (Fig. 9b). The same device was later

used when studying conformational changes in large DNA upon interaction with DNA-binding proteins (Sharma *et al.*, 2020; Jiang *et al.*, 2021a).

#### Handling ultralong DNA

In the use of nanofluidic channels for ODM applications, discussed in detail below, the size of the DNA of interest can pose experimental challenges. Introducing DNA of genomic size to a nanosized channel is associated with a significant entropic barrier, and coils of large DNA molecules tend to entangle and clog the channel entrance. An approach to promote DNA loading into nanochannels and facilitate DNA entering in an unfolded state with one end first is to include an entropic gradient in the chip design.

Physical barriers such as pillar structures, that gradually increase the confinement, provide pre-stretching of the DNA and reduce the thermodynamic cost (Cao *et al.*, 2002a; Wang *et al.*, 2015). Lam *et al.* (2012) applied this approach to genome mapping in a nanofluidic device that contained a region with channels of intermediate width and physical barriers between the feeding microfluidic channel and the nanochannel array (Fig. 8e).

Another concern to address when long, genomic DNA is confined to nanofluidic channels and visualized using fluorescence microscopy is that the size of the DNA molecule might exceed the field of view of the camera at sufficient resolution. By designing the channels in a meandering fashion (Fig. 8f) Freitag *et al.* circumvented this issue (Freitag *et al.*, 2015). In this study, a single molecule of an intact 5.7 Mbp *Schizosaccharomyces pombe* (*S. pombe*) chromosome was stretched, at an extension of 50% of its contour length to 1 mm, in a meandering nanochannel and visualized in a single field of view.

### CLiC (Convex Lens-induced Confinement)

In most nanofluidic devices, the lid is permanently bonded to the bottom of the device. In 2010, Leslie *et al.* (2010) introduced the concept of Convex Lens-induced Confinement (CLiC) microscopy, where nanoscale confinement can be repeatedly formed. The principle of CLiC relies on a convex lens pushing the lid of a chamber, forcing the lid to come in close proximity to the bottom of the chamber, thereby confining any molecules present in the solution (Berard *et al.*, 2013). In the first version, both top and bottom surfaces of the chamber were unmodified whereas in later studies the bottom surface was patterned with nanoscale features into which long DNA is forced as the chamber is squeezed by the convex lens (Fig. 9c) (Berard *et al.*, 2014). The nanoscale confinement leads to stretching of long DNA and the degree of stretching can be tailored by varying the distance between the lid and the bottom of the chamber.

The concept is compatible with several nanofluidic assays such as partially confining the DNA in pits, as well as ODM. An extension of the latter was the demonstration of a lab-on-a-chip for single-cell analysis, including cell lysis and DNA stretching in a single device (Mahshid *et al.*, 2015). By combining the CLiC procedure with electrophoresis, an increased number of molecules can be confined in the observation volume and an enhanced degree of stretching can be achieved (Ahamed *et al.*, 2016). The fact that the chamber can be repeatedly squeezed, and that the distance between the lid and bottom can be adjusted at will, makes it possible to change the solution surrounding the molecules under study. This was demonstrated by changing the ionic strength of the solution, which strongly affects DNA stretching, and further by adding cationic surfactants that condense DNA and restriction enzymes that digest DNA (Henkin *et al.*, 2016). CLiC has in more recent years been implemented in combination with other nanoscale features, such as nanopit arrays, allowing for other types of studies on DNA, in particular supercoiled DNA (Scott *et al.*, 2018, 2019; Shaheen *et al.*, 2022).

### Passivation

Due to the extreme surface to volume ratio in a nanofluidic device, even minor tendencies of non-specific binding to the channel walls can cause severe difficulties, with molecules getting stuck to the surface or clogging the channels. This is generally not a problem when studying DNA alone and using devices fabricated in

hydrophilic materials like fused silica, as the surface becomes negatively charged when the channels are filled with aqueous buffer, thereby repelling the negatively charged DNA. However, when including DNA-binding ligands or proteins, often positively charged, surface interactions become an issue and the literature provides several examples of various strategies to overcome these interactions.

Using an inert protein, like BSA, to saturate the surface before the experiment, or to include it at high concentration in the reaction buffer, is a common strategy for passivation of microfluidic channels that has been used also for nanochannels (Riehn *et al.*, 2005; Wang *et al.*, 2005; Roushan *et al.*, 2014, 2018), sometimes in combination with the non-ionic detergent Nonidet P-40 (Streng *et al.*, 2009; Lim *et al.*, 2013). Polyvinylpyrrolidone has been used as a surface passivation agent in the sample buffer (Lim *et al.*, 2013; Liu *et al.*, 2020) and addition of anionic surfactants like SDS can provide shielding of positive charges of proteins, thereby reducing non-specific binding to the channels (Öz *et al.*, 2020). Lipid bilayers can be used to effectively passivate nanofluidic structures, as demonstrated by Persson *et al.* (2012) and used in several subsequent studies (Frykholm *et al.*, 2014; Fornander *et al.*, 2016; Öz *et al.*, 2019; Sharma *et al.*, 2020). Importantly, the use of a small fraction of fluorescent lipids in the bilayers makes it possible to follow the passivation process and to investigate the integrity of the bilayer before the experiments are started. Recently, the use of a combination of dopamine and methoxypoly(ethylene glycol) for nanochannel passivation was reported (Liu *et al.*, 2020).

### Optical DNA mapping

ODM is an umbrella term for methods that allow visualization of intact DNA molecules, up to Mbp in size, to obtain sequence information with approximately kbp resolution. The length scales covered by ODM perfectly match the gap between commonly used DNA analysis methods such as fluorescence *in-situ* hybridization (chromosomal level) and DNA sequencing (base pair level). In ODM the DNA needs to be stretched, which can be done either on a glass surface by molecular combing (Bensimon *et al.*, 1994; Michalet *et al.*, 1997; Neely *et al.*, 2011) or in nanofluidic channels (Müller and Westerlund, 2017; Jeffet *et al.*, 2021b), and visualized using a fluorescence microscope. Stretching the DNA by confinement provides uniform stretching and the extension of the molecule along the channel scales linearly with the contour length of the DNA (Tegenfeldt *et al.*, 2004), thus facilitating direct extraction of sequence information from specifically labeled molecules. This makes nanofluidic channels an attractive platform for ODM. Throughput can easily be increased by parallelized systems with arrays of nanofluidic channels (Lam *et al.*, 2012) and the introduction of a commercialized platform for ODM using nanochannels (see section 'Recent applications of optical DNA mapping') has led to an increasingly widespread use of this application. In this chapter we will present ODM with focus primarily on the methodological aspects and only briefly discuss recent studies using the methodologies for high-throughput genomic analysis.

In order to access information about the underlying DNA sequence using ODM, different labeling schemes have been developed to generate a sequence-specific pattern along the extended DNA molecule. Initial efforts in the field were made by Schwartz *et al.* (1993), who used restriction enzymes to generate sequence-specific double-stranded breaks on DNA molecules

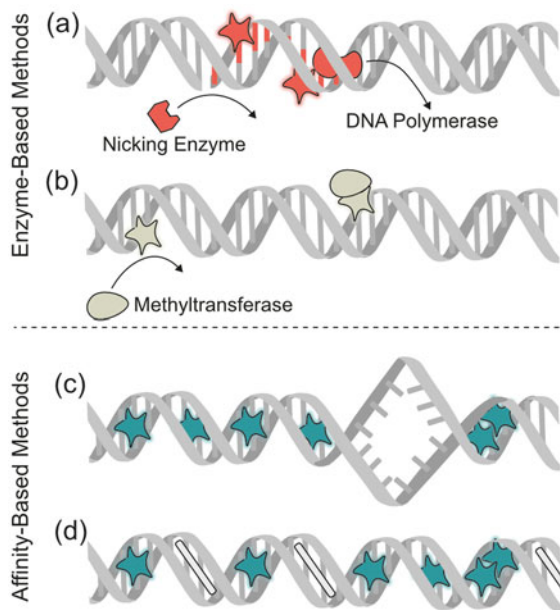


**Fig. 10.** Schematic illustration of the main optical DNA mapping labeling approaches: enzyme-based labeling methods including nick labeling (a) and methyltransferase-based labeling (b), and affinity-based methods including denaturation mapping (c) and competitive binding-based labeling (d).

when trapped in agarose gels. Present labeling approaches that are compatible with nanochannel-based analysis can be divided into two main groups, enzyme-based labeling, and affinity-based labeling (Fig. 10).

### Enzyme-based labeling

Sequence-specific labeling of DNA using enzymes can be performed in different ways. In 2007 Jo *et al.* (2007) introduced nick labeling, where nicking enzymes were used to visualize sequence-specific sites along the DNA (Fig. 11a). In short, a nicking enzyme creates a single-stranded break in the DNA at a recognition site, typically 4–7 bp in size and specific for the enzyme used. The nick is then repaired by a processive DNA polymerase that incorporates fluorescently labeled nucleotides and the position(s) of these labels can be mapped as the DNA is stretched. The contour of the DNA is visualized by staining the backbone of the DNA molecule, typically with the bis-intercalating dye YOYO-1. Several additions have been made to expand the nick labeling toolbox, including nick-flap labeling (Das *et al.*, 2010), dual nick labeling (Hastie *et al.*, 2013), and highly specific Cas9-based labeling strategies (McCaffrey *et al.*, 2016; Zhang *et al.*, 2018; Abid *et al.*, 2020; Uppuluri *et al.*, 2021).

Nick-flap labeling utilizes a DNA polymerase that lacks exonuclease activity and displaces the nucleotides at the nicking site instead of removing them, generating a single-stranded DNA flap. In this way, dual-labeling can be achieved, with the nicking site labeled by incorporation of fluorescently labeled nucleotides, and the single-stranded DNA flap labeled using a complementary, labeled oligonucleotide (Das *et al.*, 2010). Another approach to obtain dual labels is to run the nick labeling reaction twice, using two different restriction enzymes and an intermediate purification step, as was first demonstrated by Hastie *et al.* (2013).

A main limitation of traditional nicking enzymes is the limited specificity (4–7 bp). McCaffrey *et al.* addressed this issue by using

a CRISPR/Cas9-based approach, which provides a 20 bp recognition site that can be designed at will (McCaffrey *et al.*, 2016). The enzyme used was a mutated version of Cas9, a Cas9 nickase known as Cas9n or Cas9 D10A, that only nicks the DNA at the target site instead of making a double-stranded cut. Cas9-mediated nick labeling can be combined with traditional enzymatic nick labeling, to create multicolor optical maps and enable both global sequence motif mapping and labeling directed specifically to a sequence of interest, which has found applications in structural variation analysis and telomere characterization (McCaffrey *et al.*, 2016, 2017; Levy-Sakin *et al.*, 2019; Young *et al.*, 2020). Uppuluri *et al.* (2021) recently presented another multicolor labeling approach by combining Cas9-mediated nick labeling and the enzymatic direct labeling technology from BioNano Genomics (see section ‘Recent applications of optical DNA mapping’). They validated the usefulness of their methodology by quantifying copy numbers of D4Z4 repeats on chromosome 4q, detecting long non-interspersed elements 1 (LINE-1) insertions, and estimating telomere lengths. The specificity and extended use of Cas9-based labeling was further demonstrated by Abid *et al.* (2020), who identified differences between two genomes at single-base resolution, utilizing the fact that the CRISPR/Cas9 system has a strong requirement for the proto-spacer adjacent motif following the 20 bp recognition site. They also showed how mapping patterns can be customized by using a set of multiple sgRNAs of custom design in Cas9-mediated nick labeling. In line with the approach of McCaffrey *et al.* (2016), Zhang *et al.* (2018) utilized a dead, fluorescently labeled, Cas9 enzyme which only binds to DNA without cutting any of its strands, to visualize specific sequence motifs with high precision.

Sequence-specific labels can also be introduced using methyltransferases (Klimasauskas and Weinhold, 2007; Lukinavicius *et al.*, 2007). The methyltransferase recognizes a specific sequence (typically 4 bp) and attaches a synthetic co-factor at the site. The co-factor can either be pre-labeled with a fluorophore, or the fluorophore can be attached in a subsequent reaction. The short recognition site of a methyltransferase has been used to generate dense labels, so-called amplitude modulation profiles, along the DNA backbone (Grunwald *et al.*, 2015) and methyltransferase-based labeling was utilized to obtain high-resolution optical maps also by Jeffet *et al.* (2016). By combining nick labeling protocols with methyltransferase-based labeling hybrid genetic/epigenetic maps, providing both genomic and methylation profiles simultaneously, can be obtained, as illustrated by Sharim *et al.* (2019) and Gabrieli *et al.* (2022).

Besides nick labeling and methyltransferase-based labeling, there are also other enzymatic reactions that can be used to obtain specific labeling for extracting information beyond the DNA sequence. Examples include labeling of DNA hydroxymethylation (Michaeli *et al.*, 2013; Gilat *et al.*, 2017; Gabrieli *et al.*, 2018) and DNA damage (Zirkin *et al.*, 2014; Müller *et al.*, 2019; Torchinsky *et al.*, 2019).

### Affinity-based labeling

In contrast to enzyme-based labeling strategies, affinity-based labeling does not rely on any enzymatic reactions to generate the sequence-specific pattern on DNA. Instead, affinity-based labeling relies either on the difference in melting temperature of AT and GC base pairs, so-called denaturation mapping (Reisner *et al.*, 2010), or on molecules with a sequence preference when

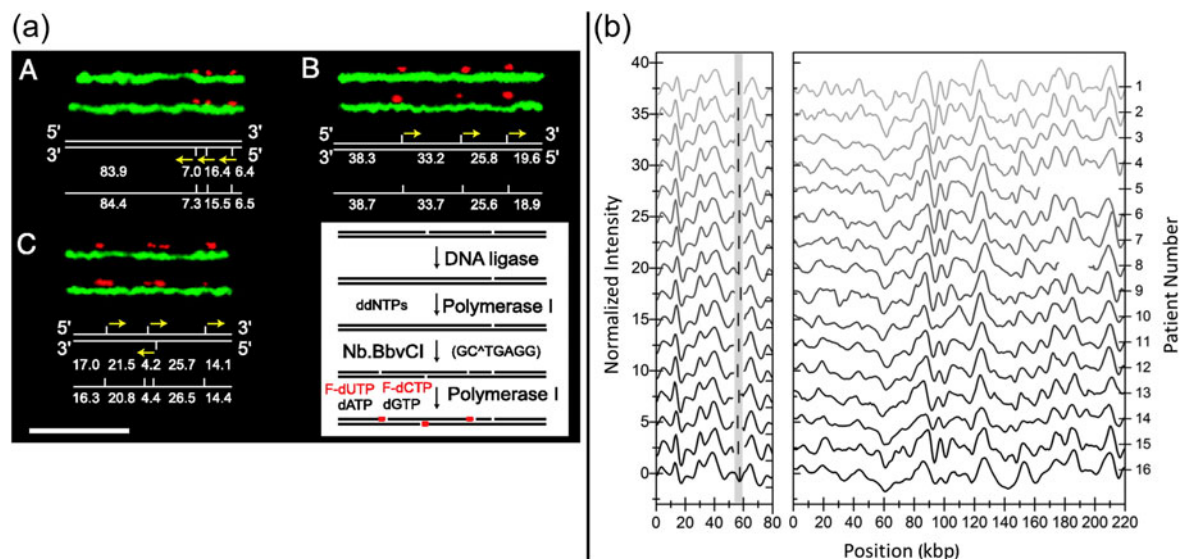


**Fig. 11.** (a) Optical maps of nick-labeled BAC molecules, 113.7 kb (A), 116.8 kb (B), and 82.5 kb (C) in size. Inset (bottom right) shows schematic overview of the nick-labeling procedure: Prior to labeling, inherent nicks are repaired or disabled using ligase and polymerase incorporation of ddNTPs. A nicking enzyme creates a single-stranded break in the DNA at a recognition site that is subsequently repaired and labeled by incorporation of fluorescently labeled dNTPs. In the fluorescence images (A–C) the DNA backbone, visualized by staining with YOYO-1, is shown in green, whereas nick-labeled sites are shown in red. Expected labeling patterns (measured in kilobases) from the sequence and maps constructed from analyzed molecules are indicated below each molecule. Scale bar is 10  $\mu$ m. Reproduced from Jo *et al.* (2007), © 2007 National Academy of Sciences. (b) Plasmids from patient isolates in a hospital outbreak of antibiotic multi-resistant bacteria characterized using ODM. The intensity profiles were generated using competitive binding-based mapping in combination with CRISPR/Cas9 restriction to detect the antibiotic resistance gene. The isolates contained two plasmids and the location of the antibiotic resistance gene on the smaller plasmid is indicated by the vertical line in the shaded region (left). ODM could reveal deletions in the larger plasmid in three of the isolates (patients 3, 5, and 8; right). All intensity profiles are shifted vertically for clarity. Reproduced from Bikkarolla *et al.* (2019), © 2019 (Bikkarolla *et al.*, 2019) under Creative Commons CC BY 4.0.

binding to DNA, such as in competitive binding-based approaches (Nyberg *et al.*, 2012).

Developed by Reisner *et al.* (2010), denaturation mapping utilizes the difference in melting temperature between GC base pairs, connected by three hydrogen bonds, and AT base pairs, connected by two hydrogen bonds. The entire contour of the DNA is stained with YOYO-1 prior to carefully raising the temperature to a level where AT base pairs melt, with subsequent YOYO-1 dissociation, while GC base pairs remain intact, with YOYO-1 still bound. As a result, the emission intensity will be bright in GC-rich regions, and dark in AT-rich regions, along the extended DNA molecule. One advantage of denaturation mapping is that it can be done either on-chip (Reisner *et al.*, 2010; Welch *et al.*, 2012) or prior to sample loading (Marie *et al.*, 2013; Łopacińska-Jørgensen *et al.*, 2017). The most recent studies using denaturation mapping have been focused on stretching very long DNA molecules by hydrodynamic flow in a shallow nanoslit. In this way, structural variations in human DNA were identified (Marie *et al.*, 2018).

With competitive binding-based mapping, it is possible to circumvent both the need for enzymatic reactions (enzymatic labeling approaches), as well as precise temperature control (denaturation mapping). DNA is instead stained by addition of a non-selective, fluorescent dye, such as YOYO-1, and a sequence-selective, non-fluorescent molecule, such as the AT-selective netropsin, mixed at a pre-defined ratio (Nyberg *et al.*, 2012; Nilsson *et al.*, 2014). Netropsin will block the AT-sites from YOYO-1, rendering an emission intensity profile, which, as for denaturation mapping, will appear dark in AT-rich regions, and bright in GC-rich regions. The use of other fluorescent dyes, such as TOTO-3, and sequence-selective molecules, such as the GC-selective actinomycin D, in competitive binding-based optical mapping has also been reported

(Esmek *et al.*, 2021). Moreover, Lee *et al.* (2018a) demonstrated how a fluorescent TAMRA-polypyrrole could be used for AT sequence visualization on DNA molecules without the need of an intercalating dye, relying on the TAMRA-polypyrrole itself to generate the intensity profile.

Overall, there are advantages and disadvantages of all the labeling approaches described above, and different strategies will be optimal for different applications. As demonstrated by Müller *et al.* (2019), it is also possible to combine enzymatic labeling with affinity-based labeling, to obtain a dual read-out, which was recently further demonstrated by Torstensson *et al.* (2021). This principle could in the future be used to increase the specificity of ODM, as well as to combine genomic data with epigenetic information.

### Recent applications of optical DNA mapping

ODM was commercialized by BioNano Genomics in 2012. Their instruments Irys<sup>®</sup> and Saphyr<sup>®</sup> rely on enzyme-based labeling in combination with nanofluidic chips with automated sample loading, image acquisition, and data analysis. The technology initially relied on nick labeling, but recently an enzymatic protocol for direct labeling of a 6 bp recognition site was introduced, with improved DNA integrity during the labeling procedure that results in longer molecules. The system has been used for a variety of applications including *de novo* assembly of complex genomes as well as for studying genetically linked diseases.

Levy-Sakin *et al.* (2019) used ODM on the BioNano Genomics platform to investigate large structural variations across the genomes of 154 individuals from 26 different populations. They were able to identify an abundance of large insertions and deletions, in many cases flanked by repetitive elements difficult to

resolve by short-read sequencing, and the presence of population-specific structural variations patterns. By including Cas9-mediated nick-labeling in the assay they could also characterize acrocentric chromosome p-arms and the study highlights how ODM can be useful in characterizing complex regions such as subtelomeric and pericentromeric areas. Young *et al.* (2020) undertook a comprehensive analysis of the subtelomere structure and variation in human genomes, by performing whole-genome ODM of the same sample set. Wu *et al.* (2019) used ODM in combination with ultrastructural imaging and computational analysis of whole-genome sequencing data to demonstrate the structure of extrachromosomal DNA in humans, DNA which is increasingly associated with oncogenes. The organization of extrachromosomal DNA was also studied by Luebeck *et al.* (2020), who developed a computational method, AmpliconReconstructor (AR), for integrating ODM from the BioNano Genomics platform with next-generation sequencing to resolve focal copy number amplification of oncogenes. Gabrieli *et al.* (2018) combined the enzyme-based ODM technology of BioNano Genomics with labeling of epigenetic 5-hydroxymethylcytosine (5-hmC) marks. The genetic/epigenetic assay allowed sensitive quantification of 5-hmC marks in blood at the single DNA molecule level. Sharim *et al.* (2019) utilized an enzymatic labeling reaction, distinguishing methylated from non-methylated cytosines, in combination with nick labeling to create hybrid genetic/epigenetic genomic maps, enabling identification of methylation patterns across the genome.

Marie *et al.* (2018) demonstrated how denaturation mapping could be combined with on-chip lysis and DNA extraction of single cells, allowing mapping of structural variations at the single DNA molecule level. Competitive binding-based ODM has recently found applications within bacterial diagnostics. Müller *et al.* (2020) demonstrated how competitive binding-based ODM could be used to identify bacteria with high precision in both complex mixtures as well as from uncultivated urine samples, circumventing the time-consuming step of bacterial cultivation prior to diagnosis. ODM based on competitive binding has also been used for identification and tracing of bacterial plasmids related to antibiotic resistance (Nyberg *et al.*, 2016; Müller *et al.*, 2016b). Utilizing the highly specific CRISPR/Cas9 system, the same research group developed an assay to detect antibiotic resistance genes on single plasmid molecules. By targeting the gene of interest, circular plasmids carrying that specific gene can be linearized by Cas9, and by observing where linearization occurred, genes could be detected with high precision and reliability (Müller *et al.*, 2016a). This plasmid typing, using competitive binding-based mapping in combination with CRISPR/Cas9 restriction, was applied by Bikkarolla *et al.* (2019) to trace and characterize plasmids from an hospital outbreak of antibiotic multi-resistant bacteria (Fig. 11b), by Lindblom *et al.* (2019) to investigate possible transfer of plasmids carrying extended-spectrum  $\beta$ -lactamase genes in sequential Enterobacteriaceae infections, and by Lin *et al.* (2020) as a tool to detect clonal spread of multidrug-resistant bacteria in a hospital setting.

### Outstanding challenges

The commercialization of ODM in nanochannels has led to an increased accessibility of this application. The available platform is capable of very high-throughput mapping of the human genome, resulting in genome maps with very high coverage.

The main challenges in the field are therefore rather linked to other aspects of the methodology, such as sample preparation, which is a complex and time-consuming process that remains a bottleneck. An important future direction for DNA mapping would be to combine sample preparation and mapping in a single device, thus minimizing the hands-on manipulation necessary to obtain the optical DNA maps. An ultimate goal of this procedure would be to perform ODM of single cells in such a device, to reveal genetic differences between cells.

Another important challenge is to maximize the information obtained from the DNA map. One approach to this is to increase the genetic information output, by for example combining multiple labeling enzymes or combining enzyme-based and competitive binding-based labeling schemes. The latter has recently been demonstrated (Torstensson *et al.*, 2021), as briefly discussed above. Alternatively, labeling to obtain genetic information can be combined with other types of labels, such as epigenetic markers (Sharim *et al.*, 2019; Margalit *et al.*, 2020; Gabrieli *et al.*, 2022) or labeling of DNA damage (Müller *et al.*, 2019), thereby adding an additional layer of information to the optical DNA map. The development of labels that can be used to obtain such additional information that is not yet accessible remains a challenge in ODM.

### DNA-protein interactions

To study DNA-protein interactions using nanofluidic channels is an attractive alternative to conventional single molecule manipulation techniques like optical or magnetic tweezers, as the use of channels circumvents the need to tether the DNA molecule to beads or surfaces, which poses limitations in the type and size of DNA that can be studied and/or preclude investigations of events taking place at the ends of the DNA molecule. Nanofluidic channels can also, similarly to other techniques, be used to characterize proteins that affect the physical properties of DNA. The first examples of DNA-protein interactions investigated using nanochannels were reported in 2005, and include the demonstration of restriction mapping in nanochannels (Riehn *et al.*, 2005) and a study of sequence-specific binding of the LacI repressor to DNA (Wang *et al.*, 2005). Although the potential for studying DNA-protein interactions in nanofluidic channels is as great as that of studying DNA itself, the progress in this field has been significantly slower, possibly hampered by the challenge of avoiding non-specific binding to the channel walls, as discussed above (section 'Passivation').

In the following sections we will review studies on (i) proteins that compact DNA; (ii) filamentous DNA-protein complexes; (iii) proteins interacting with DNA ends; and (iv) other DNA-protein interactions (Fig. 12). The main goal is to highlight the usefulness of nanochannels for studying DNA-protein interactions, but we will also point out important biophysical insights that the studies have provided.

### DNA compacting proteins

In all living cells, compaction of DNA is essential for organization of the genetic material and serves several purposes. By interactions with different proteins the DNA can be densely packed, allowing large amounts of DNA to fit into small environments. A condensed structure also provides protection of DNA from degradation and enables regulation of gene expression. Given the importance of these processes, studying proteins that act to



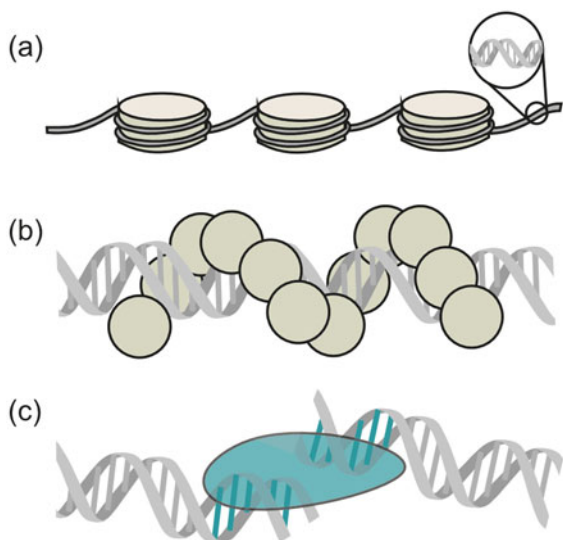


**Fig. 12.** Schematic illustration of different types of DNA-protein interactions that have been investigated by the use of nanofluidic devices: (a) protein-induced compaction of DNA (discussed in section ‘DNA compacting proteins’); (b) filamentous DNA-protein complexes (discussed in section ‘Filamentous DNA-protein complexes’); (c) proteins interacting with the ends of DNA (discussed in section ‘Proteins interacting with DNA ends’).

compact DNA and their effect on the physical properties and the structure of DNA is highly interesting and we will discuss below several examples of such studies using nanofluidic channels.

### Chromatin

Eukaryotic chromatin is comprised of DNA wrapped up on histone protein complexes, forming a densely packed structure that enables fitting the meter-long DNA in each cell into the cell nucleus. The structure of chromatin DNA plays a crucial role in gene expression and silencing and is therefore subject to heavy regulation, to a large extent governed by epigenetic modifications on the histone tails. To study linearized chromatin fibers and map genetic and/or epigenetic modifications is thus of great interest and nanofluidic channels could potentially be well suited for this purpose.

Streng *et al.* reported the first study of chromatin stretched in nanochannels (Streng *et al.*, 2009), where the chromatin used was reconstituted from a commercially available, unfractionated whole histone mixture on blunt-ended  $\lambda$ -DNA that was fluorescently labeled using YOYO-1. The extension of chromatin (in  $80 \times 80 \text{ nm}^2$  channels) was compared to that of bare DNA and chromatin was found to be 2.5 times more compact. However, the authors discuss that the chromatin was probably not in the form of condensed 30 nm fibers but rather a disordered 10 nm fiber with heterogeneous linker lengths, and physical parameters for this non-homogeneous chromatin could be given as rough estimates only.

More recently, Basak *et al.* (2020) investigated the compaction, dynamics, and internal motion of nanoconfined chromatin fibers. They used over-expressed, refolded, and purified histone octamers to reconstitute chromatin on T4-DNA, and nanofluidic devices with two different degrees of confinement ( $50 \times 70 \text{ nm}^2$  and  $120 \times 130 \text{ nm}^2$ , respectively). The compaction of DNA was followed by monitoring the extension of bare T4-DNA and

chromatin fibers formed with an octamer loading of 50 or 100%, respectively, when confined to nanochannels (Fig. 13a). The reconstituted chromatin fibers were found to not achieve a fully compacted state and fluctuations between relatively more and less open configurations were observed. The internal motion of DNA was further investigated through analysis of fluorescence correlation, from which it was deduced that this motion is governed mainly by the dynamics of uncompressed linker DNA.

Identification of histone tail modifications using fluorescent antibodies on chromatin stretched in nanochannels was demonstrated by Lim *et al.* (2013). In this study, chromatin was reconstituted from calf thymus, HeLa core, and chicken erythrocyte histones and antibodies detecting trimethylation of lysine 4 and acetylation of lysine 9, respectively, on histone 3 (H3) was used to monitor histone modifications. The ratio between these modifications varies among chromatin origins and discrimination between the three histone samples was demonstrated. Channels wider than traditionally used for DNA analysis ( $200 \times 200 \text{ nm}^2$ ), resulting in moderate stretching, were used in this study to avoid stripping of histones from the DNA and antibody aggregation.

Another approach to overcome the risk of stripping the histones off the DNA was presented by Matsuoka *et al.* (2012), who used an elastomeric nanochannel device where the channel dimensions can be adjusted post introduction of the chromatin. The chromatin in this study was isolated from HeLa cells and by co-staining with DAPI and antibodies against methylated histone H3 and acetylated histone H4, respectively, the authors were able to visualize chromatin condensation and localization of epigenetic marks on the linearized chromatin. The study points out several advantages of using nanochannels for chromatin analysis: no extra chemistry is required to stretch the chromatin, chromatin extracted from cells can be studied, and multicolor staining enables analysis of several epigenetic markers simultaneously. The latter, together with the single chromatin approach, is crucial for rare samples.

### Bacterial nucleoid-associated proteins

The bacterial chromosome is organized into a structure called the nucleoid, where the DNA forms nucleoprotein complexes with several proteins referred to as nucleoid-associated proteins (NAPs) (Azam and Ishihama, 1999). Among the most abundant and universally conserved NAPs are the heat-stable nucleoid structuring protein (H-NS) and the heat unstable nucleoid structuring protein (HU) and they have both been subject to studies using nanofluidic channels.

Zhang *et al.* (2013a) studied the effect of H-NS on DNA conformation using two different set-ups of nanofluidic channels. In steady-state experiments, an array of nanochannels was used to visualize the extension of single DNA molecules, pre-incubated with H-NS, whereas a cross-channel device (Zhang *et al.*, 2013b), described in section ‘Devices for dynamic studies’, enabled monitoring the time-dependent response of DNA upon exposure to H-NS. DNA was found to elongate or condense, depending on protein concentration, ionic strength, and presence of divalent ions ( $\text{Mg}^{2+}$ ), and H-NS mediated bridging of DNA was observed.

Later, a similar study on HU was presented (Guttula *et al.*, 2018). Contrary to the findings for H-NS, nanoconfined DNA that had been pre-incubated with HU showed a decrease in extension with increasing protein concentrations, irrespective of ionic strength and buffer composition (presence of  $\text{Mg}^{2+}$  ions).

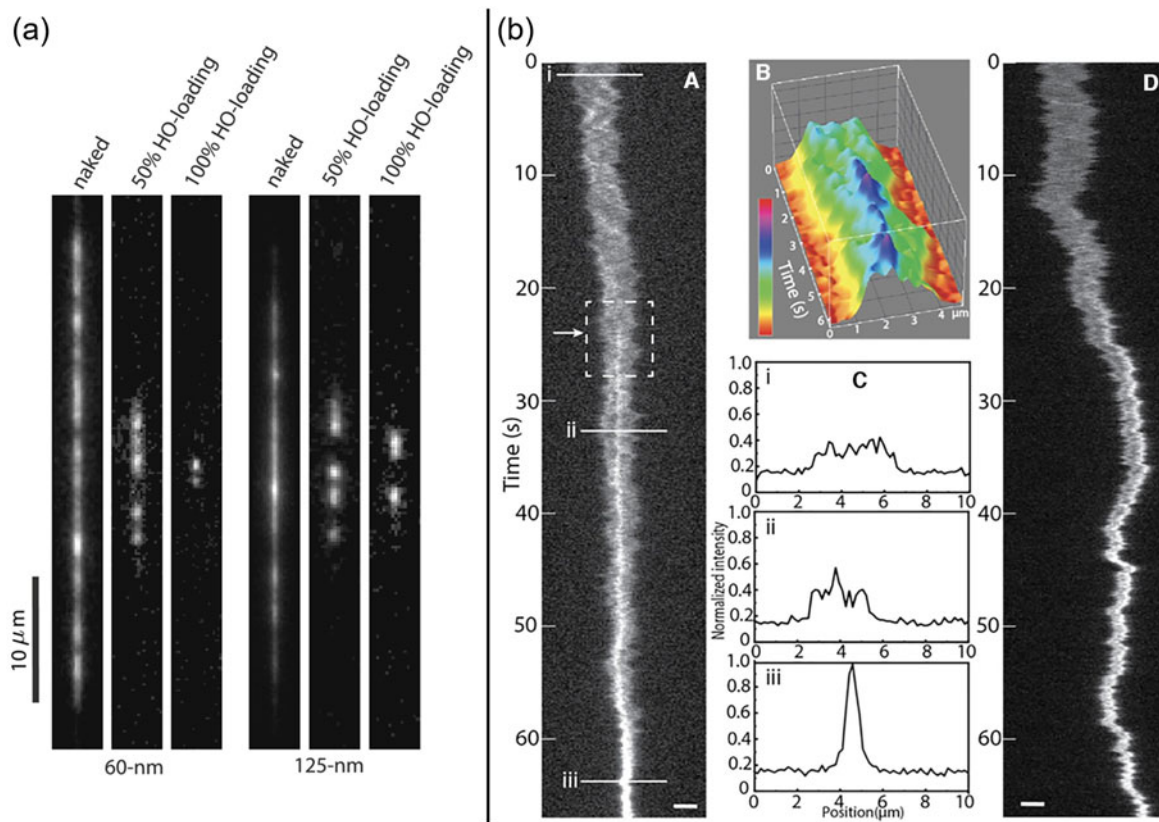


**Fig. 13.** (a) Naked T4-DNA and chromatin fibers, reconstituted with T4-DNA and two different loadings of recombinant histone octamers, stretched in nanofluidic channels. DNA is visualized by staining with YOYO-1. Chromatin fibers appear as blobs connected by strands of uncompressed DNA, and these blobs were observed to continuously reform so that the fibers fluctuate between relatively more and less open configurations. Reproduced with permission from Basak *et al.* (2020), © 2020 Biophysical Society. (b) Real-time visualization of DNA compaction upon addition of the NC protein. (A) Kymograph of YOYO-1 stained  $\lambda$ -DNA compacted and finally condensed by NC, starting in the center of the molecule (white arrow). (B) 3D surface plot showing the formation of the local condensate, at the time point corresponding to the dashed square in (A), with emission intensity color coded. (C) Normalized emission intensity profiles of DNA at the corresponding time points indicated in (A). (D) As in (A) but with the local condensate forming at the end of the DNA. The horizontal scale bars are 2  $\mu$ m. Reproduced from Jiang *et al.* (2021a), © Jiang *et al.*, (2021a) under Creative Commons CC BY-NC 4.0.

Over-threshold concentrations of protein caused DNA to collapse into a condensed conformation.

Another DNA-binding protein within the bacterial nucleoid that has been studied using nanofluidic channels is Hfq, a phylogenetically conserved and abundant bacterial protein with multiple regulatory functions related to nucleic acids metabolism. Jiang *et al.* (2015) observed compaction of DNA in the presence of wild-type, full length Hfq. The decrease in molecular extension was, just as for H-NS, explained by the propensity of Hfq to bridge distal DNA segments and at over-threshold concentrations of Hfq the DNA was found to collapse into a condensed form. In a follow-up study, truncated Hfq proteins, representing either the proposed DNA-binding C-terminal domain (Hfq-CTR) or the N-terminal region (Hfq-NTR), were investigated (Malabirade *et al.*, 2017). As a result, a proposed model for DNA binding and bridging by Hfq, where the C-terminal of the protein plays a pivotal role, with possible implications for protein-binding-related gene regulation, was presented. Recently, the effect of intramolecular DNA motion on the mobility of Hfq was investigated using a nanofluidic set-up, demonstrating a dynamic coupling between confinement-induced slowing of DNA internal motion and enhanced protein mobility (Yadav *et al.*, 2020). Subsequently, a mutant form of Hfq, lacking the C-terminal domain and having a lower DNA binding affinity, was found to

have a significantly higher mobility on DNA compared to the wild-type protein (Tan *et al.*, 2022). The mutant also demonstrated a reverse dependence on the internal motion of DNA, showing reduced protein mobility with slower internal motion.

#### Other DNA compacting proteins

Condensation and regulation of DNA accessibility are key activities also in virus life cycles. The nucleocapsid protein NC, alone and as part of the polyprotein Gag, from human immunodeficiency virus type 1 (HIV-1) has been investigated using nanochannels in two studies by Jiang *et al.* (2019, 2021a). Protein concentration-dependent compaction of nanoconfined dsDNA was demonstrated, and Gag, which has a higher binding affinity to DNA than NC alone, was shown to condense DNA at a much lower concentration than NC (Jiang *et al.*, 2019). In the same study, the ability of NC to act as a chaperone and promote annealing of complementary sequences was investigated. By using  $\lambda$ -DNA, that has 12 bp single-stranded overhangs in each end, concatemerization and circularization in the presence of NC could be observed. Recently, a further investigation of the dynamics and kinetics of dsDNA compaction induced by NC was presented (Jiang *et al.*, 2021a). A dynamic device, first described by Öz *et al.* (2019) and discussed in section 'Devices for dynamic studies', enabled real-time observation of single DNA molecules

upon addition of NC protein and the dynamics of the condensation process could thereby be followed, from locally compacted regions on the DNA to the fully condensed state (Fig. 13b). The NC-promoted annealing of complementary, single-stranded overhangs of DNA could also be visualized in real time in the dynamic device and the authors concluded that the chaperone activity is not directly correlated with the DNA condensation propensity of NC.

Another virus nucleocapsid protein studied in nanofluidic channels is the hepatitis C virus core protein (HCVcp) (Sharma *et al.*, 2020). HCVcp-induced compaction of DNA was monitored in real time, and repeated compaction and relaxation of DNA could be visualized by iterative flushing of the reaction chamber with either HCVcp (initiating compaction) or Proteinase K (releasing the DNA by degradation of the protein). It was observed that compaction preferentially starts from the ends of linear DNA, whereas for a circular substrate compaction was initiated at random positions along the contour. These observations highlight two major advantages of nanofluidic channels, over many other single-molecule techniques: as the DNA is free in solution in the channels, without any tethers, events occurring at the ends of the molecule and on circular DNA, lacking ends that make it difficult to tether, can be studied.

Stretching and visualizing single DNA–protein complexes in nanofluidic channels can provide complementary information to confirm or add detail to structural predictions from X-ray crystallography and/or models of biomolecular functions. Frykholm *et al.* (2016) studied the compaction of nanoconfined DNA by the bacteriophage protein Cox, a multifunctional transcriptional regulator in P2-like bacteriophages. Cox forms oligomeric filaments and it has been proposed from the X-ray structure that DNA can be wrapped around these filaments, in a manner similar to how histones condense DNA in eukaryotic cells. The nanofluidic experiments confirmed that Cox compacts DNA and that the binding is highly cooperative, in agreement with the postulated model. By monitoring the DNA extension at different channel widths, it was illustrated how the physical properties of the complex at low protein loads resemble those of naked DNA, whereas they are governed by the stiffer Cox-filament at higher protein coverage.

In a multimodal study by Schmitt *et al.* (2018) the structure, properties, and functions of PrgB, a surface adhesin of *Enterococcus faecalis*, were investigated. Nanofluidic channels were used to analyze PrgB binding to long DNA fragments. Compaction of DNA was observed, with full condensation of DNA at over-threshold protein concentration and deduced cooperative binding at lower concentrations. The investigation also indicated a higher affinity of PrgB for ends of DNA substrates or, alternatively, for the single-stranded overhangs present on the DNA substrates used.

### Filamentous DNA–protein complexes

A special class of DNA-binding proteins are proteins that form filaments on DNA. These filaments often have vastly different physical properties than DNA itself since the properties are governed mainly by the protein. The bacterial protein RecA and its human homolog Rad51 are key proteins in homologous recombination, a process for repairing DNA double-strand breaks (Kowalczykowski, 2015). Both RecA and Rad51 form stiff filaments on single- and double-stranded DNA. There are, however, significant differences between nucleoprotein filaments formed by the two proteins.

RecA forms homogeneous filaments along DNA and by using tapered channels, Frykholm *et al.* determined the persistence length of the filaments (Fig. 14) (Frykholm *et al.*, 2014). The filaments are stiff enough for the Odijk theory, valid when the persistence length is larger than the channel dimensions (see section ‘Odijk regime (strong confinement)’), to apply. The value obtained from the nanochannel data (1.15  $\mu\text{m}$ ) was in good agreement with the value obtained using optical tweezers (0.96  $\mu\text{m}$ ) (Hegner *et al.*, 1999), despite the different experimental set-ups where the nucleoprotein filaments were in solution without any tethering of the DNA when studied in nanochannels. This was a pioneering study as it constituted the first example of using nanofluidic channels for studying the physical properties of DNA–protein complexes.

Fornander *et al.* performed a similar study on Rad51 (Fornander *et al.*, 2016), but as the Rad51 filaments, in contrast

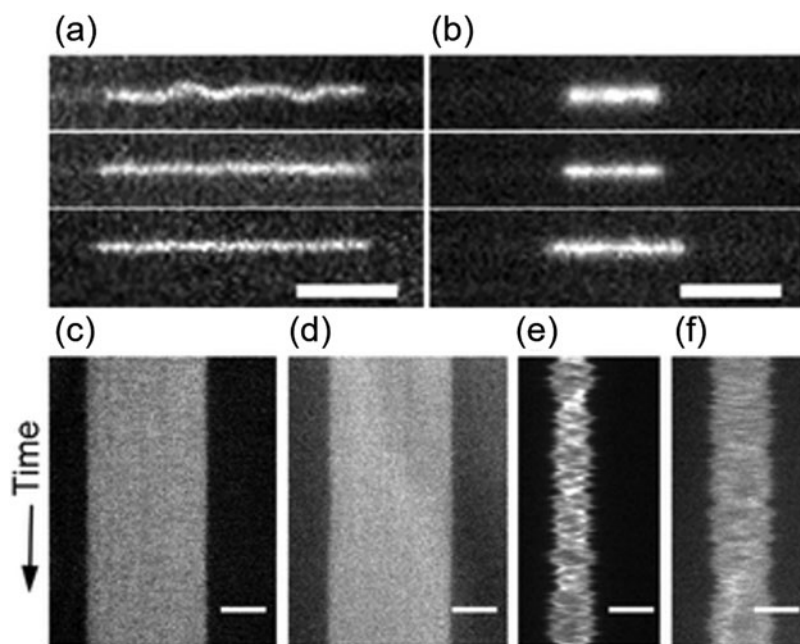


**Fig 14.** (a) Fluorescent RecA filaments formed on dsDNA studied in tapered nanochannels, imaged at three different confinements (730, 370, and 160 nm, respectively, from top to bottom). (b) dsDNA stained with YOYO-1 and imaged at the same confinements as in (a). (c–f) Kymographs for the RecA filament and the YOYO-stained DNA, respectively, in the wide (c and e) and narrow (d and f) end of the tapered channel. Each kymograph is 28 s long and aligned based on the center of mass. Scale bars correspond to 5  $\mu\text{m}$  in all images. Reproduced with permission from Frykholm *et al.* (2014), ©2014 WILEY-VCH Verlag GmbH & Co.

to the homogenous nucleoprotein filaments formed by RecA, are heterogeneous, a quantitative analysis using the Odijk theory was not as straightforward. The nucleoprotein filaments formed by Rad51 appeared in patches along the DNA, with stretches of naked DNA in between. By visualizing the filaments in the same type of tapered channels as was used in the study of RecA, Fornander *et al.* were able to characterize how the stretches of naked DNA affect the physical properties of the filaments. At weaker confinement ( $\sim 650 \times 150 \text{ nm}^2$ ) the filaments form static kinks, suggested to arise when two patches meet. At stronger confinement ( $\sim 230 \times 150 \text{ nm}^2$ ), the protein coverage on the DNA could be determined in more detail and the presence of regions of naked DNA could be confirmed. The potential biological role of the observed kinks was discussed.

### Proteins interacting with DNA ends

As discussed previously, a major advantage of using nanofluidic channels for analyzing DNA–protein complexes, compared to traditional methods where DNA is anchored in the ends, is the possibility to study reactions occurring on DNA ends and intermolecular interactions between two or more large DNA molecules. DNA ends are of interest in many different aspects, such as

in studies of telomeric DNA and in repair of DNA double-strand breaks. The use of nanofluidic channels for analysis of proteins interacting with DNA ends was first illustrated in the study on the virus nucleocapsid protein NC from HIV-1 discussed above (Jiang *et al.*, 2019), where the protein was shown to promote annealing of the 12 bp long single-stranded overhangs of long DNA molecules to form concatemers of DNA.

A first example of investigating DNA repair using nanochannels was a study of the protein CtIP by Öz *et al.* (2020). CtIP is a protein particularly known as a co-factor of MRN (Mre11-Rad50-Nbs1), a main player in the repair of double-strand breaks (Reginato and Cejka, 2020; Tisi *et al.*, 2020). Recent studies have however indicated that CtIP on its own can bind to and interact with DNA (Wilkinson *et al.*, 2019). Öz *et al.* focused on two effects of CtIP on DNA, the ability to compact DNA and the ability to bring two DNA ends in close proximity to allow annealing of broken ends. The latter was possible in this study since nanochannels enable efficient discrimination between linear and circular DNA (Alizadeheidari *et al.*, 2015). Using  $\lambda$ -DNA, that has single-stranded and complementary overhangs, the ability of CtIP to anneal ends was investigated by determining the fraction of circular DNA formed in the presence of the protein. An efficient image-collection pipeline facilitated analysis of thousands of molecules

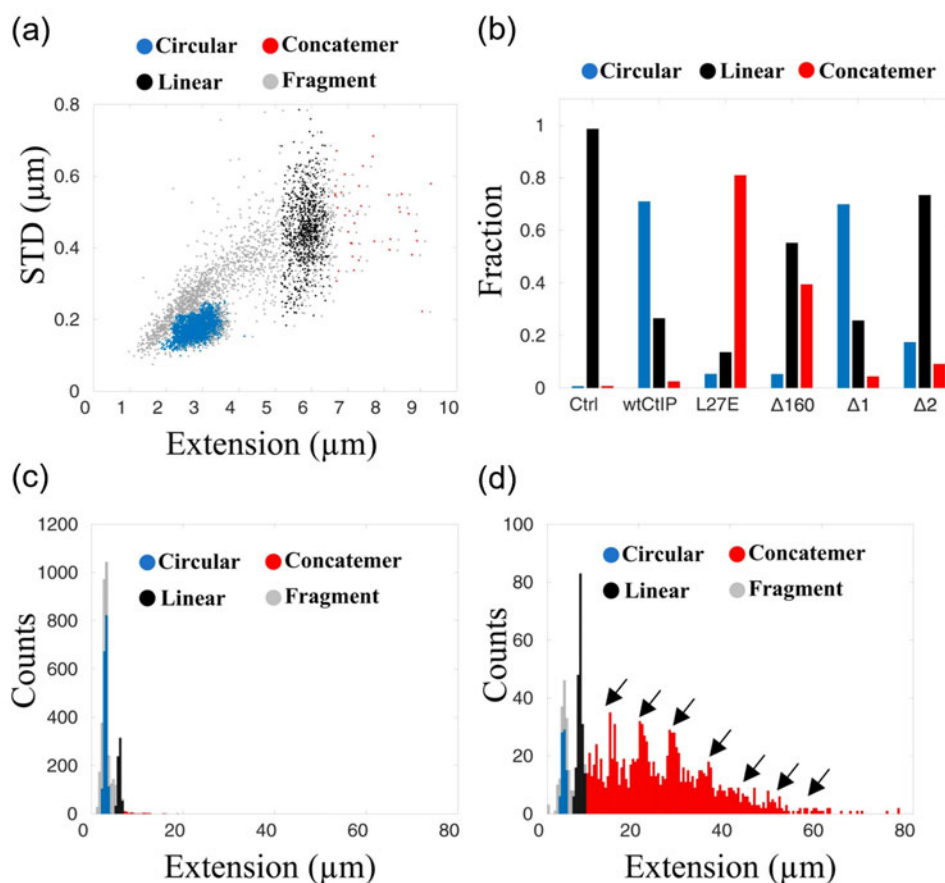


**Fig. 15.** (a) Scatterplot of molecule extension versus STD for  $\lambda$ -DNA incubated with wtCtIP, demonstrating how clustering of the dataset allowed distinguishing circularized DNA molecules (blue) from the full-size linear DNA molecules (black), concatemers (red), and linear fragments (gray). (b) The relative fractions of circular and linear complexes and concatemers differ among different CtIP mutants. The ability to bridge DNA and thereby promote circle formation was attributed to the tetrameric form of the protein. (c and d) Size histograms of molecule extension for  $\lambda$ -DNA incubated with wtCtIP (c) and mutant CtIP<sub>L27E</sub> (d), respectively. For the CtIP<sub>L27E</sub> mutant, lacking tetramer formation ability, DNA circularization is reduced and concatemerization is enhanced, compared to wtCtIP. Reproduced from Öz *et al.* (2020), © Öz *et al.* (2020) under Creative Commons CC BY 4.0.

at each condition (Fig. 15). Wild-type CtIP, in tetrameric form, was demonstrated to efficiently promote circle formation and this was suggested to be due to the protein's ability to bridge DNA and force the two DNA ends to come in close proximity. The formation of circular DNA was thus used as a readout for the potential of the protein to bridge DNA for two ends to meet. Enhanced circularization was not observed in the presence of protein mutants lacking tetramer formation ability.

Non-homologous end-joining (NHEJ) is a pathway for DNA double-strand break repair. While NHEJ in eukaryotes is a process that involves many different proteins for efficient repair, bacterial NHEJ uses only two proteins (Bowater and Doherty, 2006). The homodimeric Ku finds and binds to DNA ends, and has the ability to bridge DNA ends, while Ligase D (LigD) stabilizes the bridging and ligates the two DNA ends back together. The first detailed study of bacterial NHEJ on the single DNA molecule level was performed by Öz *et al.* using nanofluidics and magnetic tweezers (Öz *et al.*, 2021). The nanofluidics experiments revealed several important details on the functions of Ku and LigD. The first observation was that Ku alone can stably bridge DNA with as few as four bases complementary overhangs. Furthermore, Ku was found to bind cooperatively to the DNA ends and the number of Ku units in the bridges varied significantly. Another important observation was the fact that Ku was still bound at the ligation site several hours after ligation was completed (Fig. 16). The authors thus suggest that *in vivo* there must be another system present to remove Ku, and potentially LigD, from the substrate when the repair process is completed.

### Other DNA-protein interactions

Nanofluidic channels have been used to investigate the physical characteristics of DNA upon interaction also with other proteins that do not fall under any of the categories discussed above. Three important examples are presented below.

The interaction between  $\alpha$ -synuclein, a protein whose assembly process into amyloid fibers is directly related to the neurodegenerative disease Parkinson's disease, and DNA has been studied by Jiang *et al.* (2018, 2021b). Using nanofluidic channels, in

combination with other biophysical methods, binding to DNA by monomeric  $\alpha$ -synuclein was confirmed and by studying the DNA-protein complex at different confinements, an increase in DNA persistence length, up to 30%, upon protein binding was observed (Jiang *et al.*, 2018). In the follow-up study, it was shown that truncation of the C-terminus of  $\alpha$ -synuclein induces differential effects on DNA depending on the extent of the truncation (Jiang *et al.*, 2021b). Upon complete C-terminus removal (residues 1–97 of  $\alpha$ -synuclein remaining) a more than 20% decrease in relative DNA extension was observed, in contrast to the increased extension observed for full-length and residue 1–119  $\alpha$ -synuclein variants.

Conformational changes of DNA upon binding of two different methyl-CpG-binding domain (MBD) proteins were investigated, using nanofluidic channels, by Liu *et al.* (2020). They observed that MeCP2 compacted DNA to less than 50% of its native extension. From atomic force microscopy experiments, the authors deduced that compaction was caused by protein-mediated bridges between distant DNA stretches, creating local loop configurations. MBD2, on the other hand, did not affect DNA configuration and no change in DNA extension was observed upon binding of either unlabeled MBD2 or ATTO-565 labeled MBD2. The authors thus conclude that MBD2, rather than MeCP2, is a promising probe for epigenetic mapping applications, targeting methylated CpG sites.

Roushan *et al.* investigated the superdiffusive motion of DNA molecules confined to nanochannels, linked to the catalytic activity of DNA-modifying enzymes (Roushan *et al.*, 2018). In the presence of T4 DNA ligase, the mismatch DNA repair protein MutS or *E. coli* DNA ligase, respectively, and the respective energetic cofactor of each enzyme (ATP for T4 DNA ligase and MutS, NAD<sup>+</sup> for *E. coli* DNA ligase), a directed motion of nanoconfined DNA was observed and characterized. Although the displacement resembles that of a motor protein, the authors suggest that a motor-like action is not taking place. Instead, they propose a kinetic model depending on an asymmetry of ionic strengths between the termini of the DNA molecule within the nanochannel, and that this ion concentration polarization is maintained by the enzymatic reaction.

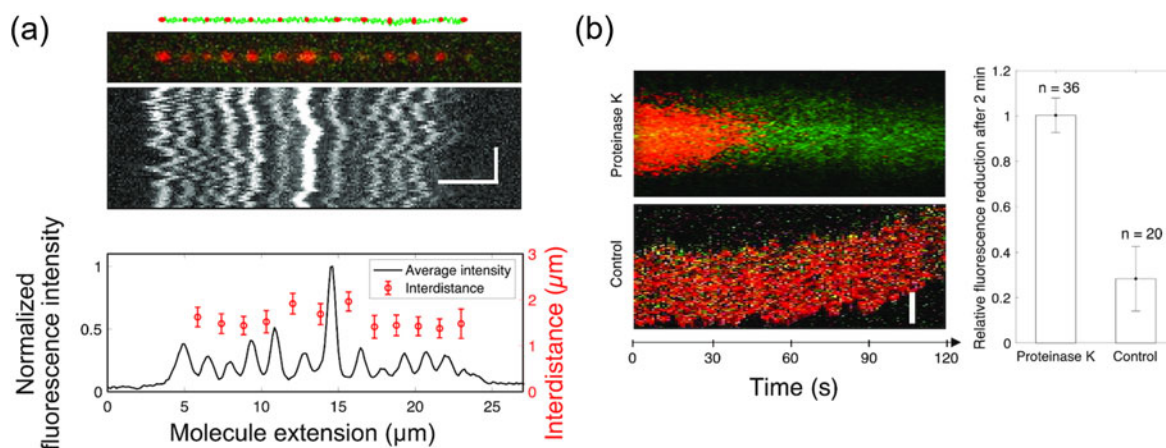


**Fig. 16.** (a) 10 kbp blunt-ended DNA molecules (stained with YOYO-1, green) bridged by Ku and covalently joined by LigD, subsequently stretched in nanofluidic channels. The locations of fluorescent Ku homodimers (red) at equal spacing correspond to the ends and junctions of the ligated DNA fragments, and the protein was observed to be stably bound post ligation. (b) The extension of YOYO-stained DNA (green) remains constant (top) after exposing the DNA-protein complex to Proteinase K, that removes the bound protein by enzymatic digestion, thereby confirming the covalent ligation. This process could be visualized in real time using a nanofluidic device that enables active buffer exchange. Minimal photobleaching is observed from the fluorescent Ku (red) in non-treated complexes during the visualization time (bottom). Reproduced from Öz *et al.* (2021), © Öz *et al.* (2021) under Creative Commons CC BY-NC 4.0.

## Outstanding challenges

In the majority of the published studies on DNA–protein interactions using nanofluidic channels the experiments were performed at equilibrium, in the sense that the protein was added to DNA outside of the device and the nanofluidic channel was used merely as a tool for visualization of the DNA–protein complexes formed. Moreover, most studies included only one protein binding to DNA. The obvious future direction for DNA–protein interaction studies using nanofluidics is thus to investigate real-time dynamics of complex reactions where more than one protein is involved, either several proteins directly interacting with DNA or indirectly through protein–protein interactions with the DNA-binding protein. Such experiments put increasing demands on device design and fabrication, as well as strategies for device passivation that need to be optimized for each specific study. The examples of device designs allowing real-time observations of DNA–protein interactions (Zhang *et al.*, 2013b; Öz *et al.*, 2019) presented in section ‘Devices for dynamic studies’ and the use of such devices to reveal reaction dynamics of simple DNA–protein systems (Zhang *et al.*, 2013a; Sharma *et al.*, 2020; Öz *et al.*, 2021; Jiang *et al.*, 2021a) are initial steps taken in this direction. Development of more advanced nanofluidic devices will make it possible to fully explore the benefits of nanofluidics for studies of DNA–protein interactions.

## Summary

The intention with this review has been to give a general overview of the usefulness of nanofluidic devices for analyzing long DNA molecules and their interactions with proteins. To do this, a thorough introduction to the polymer physics of confined DNA was initially presented. We then demonstrated how the nanofluidic devices can be tailored for the project at hand, how sequence information can be obtained from long DNA molecules by ODM and how DNA–protein interactions can be analyzed and understood using such devices.

With the development in all aspects of using nanofluidics for DNA analysis, we believe that the methodology now is ready to take a further step into broad use across scientific disciplines. The theoretical comprehension is now at a stage where it can be efficiently used for describing long DNA and its interactions in great detail. The key outstanding questions from the theory side deal with strong confinement, or, equivalently, low ionic strengths, where the neutral polymer model breaks down and the details of the DNA–wall electrostatic interactions become important (Chuang *et al.*, 2019). For the standard optical mapping analysis, the procedure has already been commercialized. We envision that an important step forward on the optical mapping track is to obtain multiple types of genetic and epigenetic information at the same time, using advanced labeling schemes along with modern imaging platforms, such as CoCoS microscopy (Jeffer *et al.*, 2021a). Another avenue to pursue is an integrated lab-on-a-chip platform aimed at high-throughput single-cell optical mapping, where initial efforts have already been made by Marie *et al.* (2018).

When it comes to using nanofluidic channels for studying DNA–protein interactions the studies presented here have paved the way for more complex analyses, where we foresee the possibility of investigating higher order interactions between DNA and several different proteins in real time with high spatial and temporal resolution, for example using super-resolution fluorescence

microscopy. One important note is that the design of the actual nanofluidic device has been underexplored and more sophisticated designs can open up for detailed biophysical analysis. These efforts should in particular focus on studies that utilize the unique features of the nanofluidic channels in that they allow DNA stretching with negligible force, studies at high throughput and studies of events occurring at the ends of long DNA.

We hope that this review will inspire researchers across disciplines to use nanofluidic devices for their research. Options are vast for DNA analysis, but the concepts can also be extended to other important topics, where recent examples in our group include analysis of biological nanoparticles (Friedrich *et al.*, 2017) and heterogeneous catalysis in the liquid phase (Levin *et al.*, 2019; Levin *et al.*, 2022).

**Financial support.** We acknowledge funding from the European Research Council, in the form of an ERC Consolidator Grant (F.W., nanoDNArepair, no. 866238), the Swedish Research Council (F.W., 2020-03400), and the US National Science Foundation (K.D.D., CBET-2016879).

**Conflict of interest.** None.

## References

- Abad E, Juarros A, Retolaza A, Merino S, Marie R and Kristensen A (2011) DNA analysis by single molecule stretching in nanofluidic biochips. *Microelectronic Engineering* **88**, 300–304.
- Abid HZ, Young E, McCaffrey J, Raseley K, Varapula D, Wang H-Y, Piazza D, Mell J and Xiao M (2020) Customized optical mapping by CRISPR–Cas9 mediated DNA labeling with multiple sgRNAs. *Nucleic Acids Research* **49**, e8.
- Ahamed MJ, Mahshid S, Berard DJ, Michaud F, Sladek R, Reisner WW and Leslie SR (2016) Continuous confinement fluidics: getting lots of molecules into small spaces with high fidelity. *Macromolecules* **49**, 2853–2859.
- Alizadehheidari M, Werner E, Noble C, Reiter-Schad M, Nyberg LK, Fritzsche J, Mehlig B, Tegenfeldt JO, Ambjörnsson T, Persson F and Westerlund F (2015) Nanoconfined circular and linear DNA: equilibrium conformations and unfolding kinetics. *Macromolecules* **48**, 871–878.
- Amin S, Khorshid A, Zeng L, Zimny P and Reisner W (2018) A nanofluidic knot factory based on compression of single DNA in nanochannels. *Nature Communications* **9**, 1506.
- Azam TA and Ishihama A (1999) Twelve species of the nucleoid-associated protein from *Escherichia coli* – sequence recognition specificity and DNA binding affinity. *Journal of Biological Chemistry* **274**, 33105–33113.
- Bakajin OB, Duke TAJ, Chou CF, Chan SS, Austin RH and Cox EC (1998) Electrohydrodynamic stretching of DNA in confined environments. *Physical Review Letters* **80**, 2737–2740.
- Basak R, Rosencrans W, Yadav I, Yan P, Berezhnoy NV, Chen Q, van Kan JA, Nordenskiöld L, Zinchenko A and van der Maarel JRC (2020) Internal motion of chromatin fibers is governed by dynamics of uncompleted linker strands. *Biophysical Journal* **119**, 2326–2334.
- Bensimon A, Simon A, Chiffaudel A, Croquette V, Heslot F and Bensimon D (1994) Alignment and sensitive detection of DNA by a moving interface. *Science* **265**, 2096–2098.
- Berard D, McFaul CMJ, Leith JS, Arsenaault AKJ, Michaud F and Leslie SR (2013) Precision platform for convex lens-induced confinement microscopy. *Review of Scientific Instruments* **84**, 103704.
- Berard DJ, Michaud F, Mahshid S, Ahamed MJ, McFaul CMJ, Leith JS, Bérubé P, Sladek R, Reisner W and Leslie SR (2014) Convex lens-induced nanoscale templating. *Proceedings of the National Academy of Sciences of the USA* **111**, 13295.
- Bhandari AB and Dorfman KD (2019) Simulations corroborate telegraph model predictions for the extension distributions of nanochannel confined DNA. *Biomicrofluidics* **13**, 044110.

- Bhandari AB and Dorfman KD** (2020) Limitations of the equivalent neutral polymer assumption for theories describing nanochannel-confined DNA. *Physical Review E* **101**, 012501.
- Bhandari AB, Reifengerger JG, Chuang HM, Cao H and Dorfman KD** (2018) Measuring the wall depletion length of nanoconfined DNA. *Journal of Chemical Physics* **149**, 104901.
- Bikkarolla SK, Nordberg V, Rajer F, Müller V, Kabir MH, Sriram KK, Dvirnas A, Ambjörnsson T, Giske CG, Navér L, Sandegren L and Westerlund F** (2019) Optical DNA mapping combined with Cas9-targeted resistance gene identification for rapid tracking of resistance plasmids in a neonatal intensive care unit outbreak. *mBio* **10**, e00347–e00319.
- Bowater R and Doherty AJ** (2006) Making ends meet: repairing breaks in bacterial DNA by non-homologous end-joining. *PLoS Genetics* **2**, e8.
- Brunet A, Tardin C, Salomé L, Rousseau P, Destainville N and Manghi M** (2015) Dependence of DNA persistence length on ionic strength of solutions with monovalent and divalent salts: a joint theory–experiment study. *Macromolecules* **48**, 3641–3652.
- Burkhardt TW, Yang Y and Gompper G** (2010) Fluctuations of a long, semi-flexible polymer in a narrow channel. *Physical Review E* **82**, 041801.
- Bustamante C, Marko JF, Siggia ED and Smith S** (1994) Entropic elasticity of lambda-phage DNA. *Science* **265**, 1599–1600.
- Cao H, Tegenfeldt JO, Austin RH and Chou SY** (2002a) Gradient nanostructures for interfacing microfluidics and nanofluidics. *Applied Physics Letters* **81**, 3058–3060.
- Cao H, Yu Z, Wang J, Tegenfeldt JO, Austin RH, Chen E, Wu W and Chou SY** (2002b) Fabrication of 10 nm enclosed nanofluidic channels. *Applied Physics Letters* **81**, 174–176.
- Chaurasiya KR, Paramanathan T, McCauley MJ and Williams MC** (2010) Biophysical characterization of DNA binding from single molecule force measurements. *Physics of Life Reviews* **7**, 299–341.
- Chen JZY** (2016) Theory of wormlike polymer chains in confinement. *Progress in Polymer Science* **54–55**, 3–46.
- Chen JZY** (2017) Conformational properties of a back-folding wormlike chain confined in a cylindrical tube. *Physical Review Letters* **118**, 247802.
- Chen JZY** (2018) Self-avoiding wormlike chain confined in a cylindrical tube: scaling behavior. *Physical Review Letters* **121**, 037801.
- Chen ZY and Noolandi J** (1992) Renormalization-group scaling theory for flexible and wormlike polymer chains. *Journal of Chemical Physics* **96**, 1540.
- Chen J, Sun L, Wang S, Tian F, Zhu H, Zhang R and Dai L** (2021) Crowding-induced polymer trapping in a channel. *Physical Review E* **104**, 054502.
- Cheong GK, Li X and Dorfman KD** (2017) Wall depletion length of a channel-confined polymer. *Physical Review E* **95**, 022501.
- Chuang HM, Reifengerger JG, Cao H and Dorfman KD** (2017) Sequence-dependent persistence length of long DNA. *Physical Review Letters* **119**, 227802.
- Chuang HM, Reifengerger JG, Bhandari AB and Dorfman KD** (2019) Extension distribution for DNA confined in a nanochannel near the Odijk regime. *Journal of Chemical Physics* **151**, 114903.
- Cifra P and Bleha T** (2012) Detection of chain backfolding in simulation of DNA in nanofluidic channels. *Soft Matter* **8**, 9022–9028.
- Clisby N** (2010) Accurate estimate of the critical exponent  $\nu$  for self-avoiding walks via a fast implementation of the pivot algorithm. *Physical Review Letters* **104**, 055702.
- Collins BE, Ye LF, Duzdevich D and Greene EC** (2014) DNA curtains: novel tools for imaging protein–nucleic acid interactions at the single-molecule level. *Methods in Cell Biology* **123**, 217–234.
- Dai L and Doyle PS** (2013) Comparisons of a polymer in confinement versus applied force. *Macromolecules* **46**, 6336–6344.
- Dai L and Doyle PS** (2018) Universal knot spectra for confined polymers. *Macromolecules* **51**, 6327–6333.
- Dai L, Ng SY, Doyle PS and van der Maarel JRC** (2012) Conformation model of back-folding and looping of a single DNA molecule confined inside a nanochannel. *ACS Macro Letters* **1**, 1046–1050.
- Dai L, van der Maarel J and Doyle PS** (2014) Extended de Gennes regime of DNA confined in a nanochannel. *Macromolecules* **47**, 2445–2450.
- Daoud M and De Gennes PG** (1977) Statistics of macromolecular solutions trapped in small pores. *Journal of Physics France* **38**, 85–93.
- Das SK, Austin MD, Akana MC, Deshpande P, Cao H and Xiao M** (2010) Single molecule linear analysis of DNA in nano-channel labeled with sequence specific fluorescent probes. *Nucleic Acids Research* **38**, e177.
- De Vlaminck I and Dekker C** (2012) Recent advances in magnetic tweezers. *Annual Review of Biophysics* **41**, 453–472.
- Dobrynin AV** (2005) Electrostatic persistence length of semiflexible and flexible polyelectrolytes. *Macromolecules* **38**, 9304–9314.
- Dorfman KD** (2010) DNA electrophoresis in microfabricated devices. *Reviews of Modern Physics* **82**, 2903–2947.
- Dorfman KD** (2018) The statistical segment length of DNA: opportunities for biomechanical modeling in polymer physics and next-generation genomics. *Journal of Biomechanical Engineering* **140**, 0208011–0208019.
- Duan C, Wang W and Xie Q** (2013) Review article: fabrication of nanofluidic devices. *Biomicrofluidics* **7**, 026501.
- Esmek FM, Bayat P, Pérez-Willard F, Volkenandt T, Blick RH and Fernandez-Cuesta I** (2019) Sculpturing wafer-scale nanofluidic devices for DNA single molecule analysis. *Nanoscale* **11**, 13620–13631.
- Esmek FM, Erichlandwehr T, Mors DHB, Czech-Sioli M, Therre M, Günther T, Grundhoff A, Fischer N and Fernandez-Cuesta I** (2021) Real time, in-line optical mapping of single molecules of DNA. *Biosensors and Bioelectronics: X* **9**, 100087.
- Feng B, Sosa RP, Mårtensson AKF, Jiang K, Tong A, Dorfman KD, Takahashi M, Lincoln P, Bustamante CJ, Westerlund F and Nordén B** (2019) Hydrophobic catalysis and a potential biological role of DNA unstacking induced by environment effects. *Proceedings of the National Academy of Sciences of the USA* **116**, 17169–17174.
- Fornander LH, Frykholm K, Fritzsche J, Araya J, Nevin P, Werner E, Cakir A, Persson F, Garcin EB, Beuning PJ, Mehlig B, Modesti M and Westerlund F** (2016) Visualizing the nonhomogeneous structure of RAD51 filaments using nanofluidic channels. *Langmuir* **32**, 8403–8412.
- Freitag C, Noble C, Fritzsche J, Persson F, Reiter-Schad M, Nilsson AN, Graneli A, Ambjörnsson T, Mir KU and Tegenfeldt JO** (2015) Visualizing the entire DNA from a chromosome in a single frame. *Biomicrofluidics* **9**, 044114.
- Friedrich R, Block S, Alizadehheidari M, Heider S, Fritzsche J, Esbjörner EK, Westerlund F and Bally M** (2017) A nano flow cytometer for single lipid vesicle analysis. *Lab on a Chip* **17**, 830–841.
- Frykholm K, Alizadehheidari M, Fritzsche J, Wiggenius J, Modesti M, Persson F and Westerlund F** (2014) Probing physical properties of a DNA-protein complex using nanofluidic channels. *Small* **10**, 884–887.
- Frykholm K, Bertsson RP, Claesson M, De Battice L, Odegrip R, Stenmark P and Westerlund F** (2016) DNA compaction by the bacteriophage protein Cox studied on the single DNA molecule level using nanofluidic channels. *Nucleic Acids Research* **44**, 7219–7227.
- Gabrieli T, Sharim H, Nifker G, Jeffert J, Shahal T, Arielly R, Levi-Sakin M, Hoch L, Arbib N, Michaeli Y and Ebenstein Y** (2018) Epigenetic optical mapping of 5-hydroxymethylcytosine in nanochannel arrays. *ACS Nano* **12**, 7148–7158.
- Gabrieli T, Michaeli Y, Avraham S, Torchinsky D, Margalit S, Schütz L, Juhasz M, Coruh C, Arbib N, Zhou ZS, Law JA, Weinhold E and Ebenstein Y** (2022) Chemoenzymatic labeling of DNA methylation patterns for single-molecule epigenetic mapping. *Nucleic Acids Research* **50**, e92.
- Gilat N, Tabachnik T, Shwartz A, Shahal T, Torchinsky D, Michaeli Y, Nifker G, Zirkin S and Ebenstein Y** (2017) Single-molecule quantification of 5-hydroxymethylcytosine for diagnosis of blood and colon cancers. *Clinical Epigenetics* **9**, 70.
- Grunwald A, Dahan M, Giesbertz A, Nilsson A, Nyberg LK, Weinhold E, Ambjörnsson T, Westerlund F and Ebenstein Y** (2015) Bacteriophage strain typing by rapid single molecule analysis. *Nucleic Acids Research* **43**, e117.
- Gu J, Gupta R, Chou C-F, Wei Q and Zenhausern F** (2007) A simple polysilsequioxane sealing of nanofluidic channels below 10 nm at room temperature. *Lab on a Chip* **7**, 1198–1201.

- Guilbaud S, Salome L, Destainville N, Manghi M and Tardin C (2019) Dependence of DNA persistence length on ionic strength and ion type. *Physical Review Letters* **122**, 028102.
- Gunther K, Mertig M and Seidel R (2010) Mechanical and structural properties of YOYO-1 complexed DNA. *Nucleic Acids Research* **38**, 6526–6532.
- Guo LJ, Cheng X and Chou C-F (2004) Fabrication of size-controllable nanofluidic channels by nanoimprinting and its application for DNA stretching. *Nano Letters* **4**, 69–73.
- Gupta D, Sheats J, Muralidhar A, Miller JJ, Huang DE, Mahshid S, Dorfman KD and Reisner W (2014) Mixed confinement regimes during equilibrium confinement spectroscopy of DNA. *Journal of Chemical Physics* **140**, 214901.
- Gupta D, Miller JJ, Muralidhar A, Mahshid S, Reisner W and Dorfman KD (2015) Experimental evidence of weak excluded volume effects for nanochannel confined DNA. *ACS Macro Letters* **4**, 759–763.
- Gupta D, Bhandari AB and Dorfman KD (2018) Evaluation of blob theory for the diffusion of DNA in nanochannels. *Macromolecules* **51**, 1748–1755.
- Guttula D, Liu F, van Kan JA, Arluison V and van der Maarel JRC (2018) Effect of HU protein on the conformation and compaction of DNA in a nanochannel. *Soft Matter* **14**, 2322–2328.
- Han M, Kim BC, Matsuoka T, Thouless MD and Takayama S (2016) Dynamic simulations show repeated narrowing maximizes DNA linearization in elastomeric nanochannels. *Biomicrofluidics* **10**, 064108.
- Hastie AR, Dong L, Smith A, Finklestein J, Lam ET, Huo N, Cao H, Kwok PY, Deal KR, Dvorak J, Luo MC, Gu Y and Xiao M (2013) Rapid genome mapping in nanochannel arrays for highly complete and accurate de novo sequence assembly of the complex *Aegilops tauschii* genome. *PLoS ONE* **8**, e55864.
- Hegner M, Smith SB and Bustamante C (1999) Polymerization and mechanical properties of single RecA-DNA filaments. *Proceedings of the National Academy of Sciences of the USA* **96**, 10109–10114.
- Heller I, Hoekstra TP, King GA, Peterman EJ and Wuite GJ (2014) Optical tweezers analysis of DNA-protein complexes. *Chemical Reviews* **114**, 3087–3119.
- Henkin G, Berard D, Stabile F, Shayegan M, Leith JS and Leslie SR (2016) Manipulating and visualizing molecular interactions in customized nanospace. *Analytical Chemistry* **88**, 11100–11107.
- Hiemenz PC and Lodge TP (2007) *Polymer Chemistry*. Hoboken: CRC Press.
- Hsieh CC, Balducci A and Doyle PS (2008) Ionic effects on the equilibrium dynamics of DNA confined in nanoslits. *Nano Letters* **8**, 1683–1688.
- Huh D, Mills KL, Zhu X, Burns MA, Thouless MD and Takayama S (2007) Tuneable elastomeric nanochannels for nanofluidic manipulation. *Nature Materials* **6**, 424–428.
- Iarko V, Werner E, Nyberg LK, Muller V, Fritzsche J, Ambjornsson T, Beech JP, Tegenfeldt JO, Mehlig K, Westerlund F and Mehlig B (2015) Extension of nanoconfined DNA: quantitative comparison between experiment and theory. *Physical Review E* **92**, 062701.
- Jeffet J, Kobo A, Su T, Grunwald A, Green O, Nilsson AN, Eisenberg E, Ambjornsson T, Westerlund F, Weinhold E, Shabat D, Purohit PK and Ebenstein Y (2016) Super-resolution genome mapping in silicon nanochannels. *ACS Nano* **10**, 9823–9830.
- Jeffet J, Ionescu A, Michaeli Y, Torchinsky D, Perlson E, Craggs TD and Ebenstein Y (2021a) Multimodal single-molecule microscopy with continuously controlled spectral resolution. *Biophysical Reports* **1**, 100013.
- Jeffet J, Margalit S, Michaeli Y and Ebenstein Y (2021b) Single-molecule optical genome mapping in nanochannels: multidisciplinary at the nanoscale. *Essays in Biochemistry* **65**, 51–66.
- Jeon C, Jung Y and Ha B-Y (2016) Effects of molecular crowding and confinement on the spatial organization of a biopolymer. *Soft Matter* **12**, 9436–9450.
- Jiang K, Zhang C, Guttula D, Liu F, van Kan JA, Lavelle C, Kubiak K, Malabirade A, Lapp A, Arluison V and van der Maarel JR (2015) Effects of Hfq on the conformation and compaction of DNA. *Nucleic Acids Research* **43**, 4332–4341.
- Jiang K, Rocha S, Westling A, Kesaramangalam S, Dorfman KD, Wittung-Stafshede P and Westerlund F (2018) Alpha-synuclein modulates the physical properties of DNA. *Chemistry - A European Journal* **24**, 15685–15690.
- Jiang K, Humbert N, Sriram KK, Lequeu T, Lin Y-L, Mely Y and Westerlund F (2019) Annealing of ssDNA and compaction of dsDNA by the HIV-1 nucleocapsid and Gag proteins visualized using nanofluidic channels. *Quarterly Reviews of Biophysics* **52**, 1–10.
- Jiang K, Humbert N, S KK, Rouzina I, Mely Y and Westerlund F (2021a) The HIV-1 nucleocapsid chaperone protein forms locally compacted globules on long double-stranded DNA. *Nucleic Acids Research* **49**, 4550–4563.
- Jiang K, Rocha S, Kumar R, Westerlund F and Wittung-Stafshede P (2021b) C-terminal truncation of  $\alpha$ -synuclein alters DNA structure from extension to compaction. *Biochemical and Biophysical Research Communications* **568**, 43–47.
- Jo K, Dhingra DM, Odijk T, De Pablo JJ, Graham MD, Runnheim R, Forrest D and Schwartz DC (2007) A single-molecule barcoding system using nanoslits for DNA analysis. *Proceedings of the National Academy of Sciences of the USA* **104**, 2673–2678.
- Jones JJ, van der Maarel JR and Doyle PS (2011) Effect of nanochannel geometry on DNA structure in the presence of macromolecular crowding agent. *Nano Letters* **11**, 5047–5053.
- Jun S, Thirumalai D and Ha BY (2008) Compression and stretching of a self-avoiding chain in cylindrical nanopores. *Physical Review Letters* **101**, 138101.
- Kang ESH, Sriram KK, Jeon I, Kim J, Chen S, Kim K-H, Kim K-H, Lee HS, Westerlund F and Jonsson MP (2022) Organic anisotropic excitonic optical nanoantennas. *Advanced Science* **9**, e2201907.
- Kim Y, Kim KS, Kounovsky KL, Chang R, Jung GY, Depablo JJ, Jo K and Schwartz DC (2011) Nanochannel confinement: DNA stretch approaching full contour length. *Lab on a Chip* **11**, 1721–1729.
- Klimasauskas S and Weinhold E (2007) A new tool for biotechnology: AdoMet-dependent methyltransferases. *Trends in Biotechnology* **25**, 99–104.
- Kounovsky-Shafer KL, Hernandez-Ortiz JP, Potamouis K, Tsvit G, Place M, Ravindran P, Jo K, Zhou S, Odijk T, De Pablo JJ and Schwartz DC (2017) Electrostatic confinement and manipulation of DNA molecules for genome analysis. *Proceedings of the National Academy of Sciences of the USA* **114**, 13400–13405.
- Kowalczykowski SC (2015) An overview of the molecular mechanisms of recombinational DNA repair. *Cold Spring Harbor Perspectives in Biology* **7**.
- Kratky O and Porod G (1949) Röntgenuntersuchung gelöster Fadenmoleküle. *Recueil des Travaux Chimiques des Pays-Bas* **68**, 1106–1122.
- Krog J, Alizadehheidari M, Werner E, Bikkarolla SK, Tegenfeldt JO, Mehlig B, Lomholt MA, Westerlund F and Ambjornsson T (2018) Stochastic unfolding of nanoconfined DNA: experiments, model and Bayesian analysis. *Journal of Chemical Physics* **149**, 215101.
- Kundukad B, Yan J and Doyle PS (2014) Effect of YOYO-1 on the mechanical properties of DNA. *Soft Matter* **10**, 9721–9728.
- Kutchoukov VG, Laugere F, Vlist WVD, Pakula L, Garini Y, Alkemade PFA and Bossche A (2003) Fabrication of nanochannels using glass to glass anodic bonding. *TRANSDUCERS '03. 12th International Conference on Solid-State Sensors, Actuators and Microsystems. Digest of Technical Papers (Cat. No.03TH8664)*, vol. 2, pp. 1327–1330 vol.1322.
- Lam ET, Hastie A, Lin C, Ehrlich D, Das SK, Austin MD, Deshpande P, Cao H, Nagarajan N, Xiao M and Kwok PY (2012) Genome mapping on nanochannel arrays for structural variation analysis and sequence assembly. *Nature Biotechnology* **30**, 771–776.
- Lee S, Kawamoto Y, Vaijayanthi T, Park J, Bae J, Kim-Ha J, Sugiyama H and Jo K (2018a) TAMRA-polypyrrole for A/T sequence visualization on DNA molecules. *Nucleic Acids Research* **46**, e108.
- Lee S, Lee Y, Kim Y, Wang C, Park J, Jung GY, Chen Y, Chang R, Ikeda S, Sugiyama H and Jo K (2018b) Nanochannel-confined TAMRA-polypyrrole stained DNA stretching by varying the ionic strength from micromolar to millimolar concentrations. *Polymers* **11**, 11010015.
- Leslie SR, Fields AP and Cohen AE (2010) Convex lens-induced confinement for imaging single molecules. *Analytical Chemistry* **82**, 6224–6229.
- Lesser-Rojas L, Sriram KK, Liao K-T, Lai S-C, Kuo P-C, Chu M-L and Chou C-F (2014) Tandem array of nanoelectronic readers embedded coplanar to a fluidic nanochannel for correlated single biopolymer analysis. *Biomicrofluidics* **8**, 016501.



- Levin S, Fritzsche J, Nilsson S, Runemark A, Dhokale B, Ström H, Sundén H, Langhammer C and Westerlund F (2019) A nanofluidic device for parallel single nanoparticle catalysis in solution. *Nature Communications* **10**, 4426.
- Levin S, Lerch S, Boje A, Fritzsche J, Sriram KK, Ström H, Moth-Poulsen K, Sundén H, Hellman A, Westerlund F and Langhammer C (2022) Nanofluidic trapping of faceted colloidal nanocrystals for parallel single-particle catalysis. *ACS Nano* **16**, 15206–15214.
- Levy-Sakin M, Pastor S, Mostovoy Y, Li L, Leung AKY, McCaffrey J, Young E, Lam ET, Hastie AR, Wong KHY, Chung CYL, Ma W, Sibert J, Rajagopalan R, Jin N, Chow EYC, Chu C, Poon A, Lin C, Naguib A, Wang W-P, Cao H, Chan T-F, Yip KY, Xiao M and Kwok P-Y (2019) Genome maps across 26 human populations reveal population-specific patterns of structural variation. *Nature Communications* **10**, 1025.
- Liao G-J, Chien F-T, Luzhbin D and Chen Y-L (2015) Entropic attraction: polymer compaction and expansion induced by nano-particles in confinement. *The Journal of Chemical Physics* **142**, 174904.
- Lim SE, Karpusenko A, Blumers AL, Streng DE and Riehn R (2013) Chromatin modification mapping in nanochannels. *Biomicrofluidics* **7**, 64105.
- Lin YL, Sewunet T, Sriram KK, Giske CG and Westerlund F (2020) Optical maps of plasmids as a proxy for clonal spread of MDR bacteria: a case study of an outbreak in a rural Ethiopian hospital. *Journal of Antimicrobial Chemotherapy* **75**, 2804–2811.
- Lindblom A, Sriram KK, Muller V, Oz R, Sandstrom H, Ahren C, Westerlund F and Karami N (2019) Interspecies plasmid transfer appears rare in sequential infections with extended-spectrum beta-lactamase (ESBL)-producing Enterobacteriaceae. *Diagnostic Microbiology and Infectious Disease* **93**, 380–385.
- Liu M, Movahed S, Dangi S, Pan H, Kaur P, Bilinovich SM, Faison EM, Leighton GO, Wang H, Williams DC Jr. and Riehn R (2020) DNA looping by two 5-methylcytosine-binding proteins quantified using nanofluidic devices. *Epigenetics & Chromatin* **13**, 18.
- Lopacińska-Jørgensen JM, Pedersen JN, Bak M, Mehrjouy MM, Sørensen KT, Østergaard PF, Bilenberg B, Kristensen A, Taboryski RJ, Flyvbjerg H, Marie R, Tommerup N and Silaharoglu A (2017) Enrichment of megabase-sized DNA molecules for single-molecule optical mapping and next-generation sequencing. *Scientific Reports* **7**, 17893.
- Luebeck J, Coruh C, Dehkordi SR, Lange JT, Turner KM, Deshpande V, Pai DA, Zhang C, Rajkumar U, Law JA, Mischel PS and Bafna V (2020) AmpliconReconstructor integrates NGS and optical mapping to resolve the complex structures of focal amplifications. *Nature Communications* **11**, 4374.
- Lukinavicius G, Lapiene V, Stasevskij Z, Dalhoff C, Weinhold E and Klimasauskas S (2007) Targeted labeling of DNA by methyltransferase-directed transfer of activated groups (mTAG). *Journal of the American Chemical Society* **129**, 2758–2759.
- Ma Z and Dorfman KD (2020) Diffusion of knots along DNA confined in nanochannels. *Macromolecules* **53**, 6461–6468.
- Ma Z and Dorfman KD (2021a) Diffusion of knotted DNA molecules in nanochannels in the extended de Gennes regime. *Macromolecules* **54**, 4211–4218.
- Ma Z and Dorfman KD (2021b) Interactions between two knots in nanochannel-confined DNA molecules. *The Journal of Chemical Physics* **155**, 154901.
- Mahshid S, Ahamed MJ, Berard D, Amin S, Sladek R, Leslie SR and Reisner W (2015) Development of a platform for single cell genomics using convex lens-induced confinement. *Lab on a Chip* **15**, 3013–3020.
- Malabirade A, Jiang K, Kubiak K, Diaz-Mendoza A, Liu F, van Kan JA, Berret JF, Arluison V and van der Maarel JRC (2017) Compaction and condensation of DNA mediated by the C-terminal domain of Hfq. *Nucleic Acids Research* **45**, 7299–7308.
- Manneschi C, Angeli E, Ala-Nissila T, Repetto L, Firpo G and Valbusa U (2013) Conformations of DNA in triangular nanochannels. *Macromolecules* **46**, 4198–4206.
- Margalit S, Avraham S, Shahal T, Michaeli Y, Gilat N, Magod P, Caspi M, Loewenstein S, Lahat G, Friedmann-Morvinski D, Kariv R, Rosin-Arbesfeld R, Zirkin S and Ebenstein Y (2020) 5-Hydroxymethylcytosine as a clinical biomarker: fluorescence-based assay for high-throughput epigenetic quantification in human tissues. *International Journal of Cancer* **146**, 115–122.
- Marie R, Pedersen JN, Bauer DLV, Rasmussen KH, Yusuf M, Volpi E, Flyvbjerg H, Kristensen A and Mir KU (2013) Integrated view of genome structure and sequence of a single DNA molecule in a nanofluidic device. *Proceedings of the National Academy of Sciences of the USA* **110**, 4893–4898.
- Marie R, Pedersen JN, Bærlocher L, Koprowska K, Pødenphant M, Sabatel C, Zalkovskij M, Mironov A, Bilenberg B, Ashley N, Flyvbjerg H, Bodmer WF, Kristensen A and Mir KU (2018) Single-molecule DNA-mapping and whole-genome sequencing of individual cells. *Proceedings of the National Academy of Sciences of the USA* **115**, 11192.
- Matsuoka T, Kim BC, Huang J, Douville NJ, Thouless MD and Takayama S (2012) Nanoscale squeezing in elastomeric nanochannels for single chromatin linearization. *Nano Letters* **12**, 6480–6484.
- McCaffrey J, Sibert J, Zhang B, Zhang Y, Hu W, Riethman H and Xiao M (2016) CRISPR-CAS9 D10A nickase target-specific fluorescent labeling of double strand DNA for whole genome mapping and structural variation analysis. *Nucleic Acids Research* **44**, e11.
- McCaffrey J, Young E, Lassahn K, Sibert J, Pastor S, Riethman H and Xiao M (2017) High-throughput single-molecule telomere characterization. *Genome Research* **27**, 1904–1915.
- Menard LD and Ramsey JM (2013) Electrokinetically-driven transport of DNA through focused ion beam milled nanofluidic channels. *Analytical Chemistry* **85**, 1146–1153.
- Metzler R, Reisner W, Riehn R, Austin R, Tegenfeldt JO and Sokolov IM (2006) Diffusion mechanisms of localised knots along a polymer. *Europhysics Letters (EPL)* **76**, 696–702.
- Michaeli Y, Shahal T, Torchinsky D, Grunwald A, Hoch R and Ebenstein Y (2013) Optical detection of epigenetic marks: sensitive quantification and direct imaging of individual hydroxymethylcytosine bases. *Chemical Communications* **49**, 8599–8601.
- Michalet X, Ekong R, Fougerousse F, Rousseaux S, Schurra C, Hornigold N, Slegtenhorst MV, Wolfe J, Povey S, Beckmann JS and Bensimon A (1997) Dynamic molecular combing: stretching the whole human genome for high-resolution studies. *Science* **277**, 1518–1523.
- Micheletti C (2022) DNA knots. In Tezuka Y and Deguchi T (eds), *Topological Polymer Chemistry: Concepts and Practices*. Singapore: Springer Nature Singapore, pp. 115–133.
- Micheletti C and Orlandini E (2012) Knotting and metric scaling properties of DNA confined in nano-channels: a Monte Carlo study. *Soft Matter* **8**, 10959–10968.
- Micheletti C and Orlandini E (2014) Knotting and unknotting dynamics of DNA strands in nanochannels. *ACS Macro Letters* **3**, 876–880.
- Müller V and Westerlund F (2017) Optical DNA mapping in nanofluidic devices: principles and applications. *Lab on a Chip* **17**, 579–590.
- Muller V, Rajer F, Frykholm K, Nyberg LK, Quaderi S, Fritzsche J, Kristiansson E, Ambjörnsson T, Sandegren L and Westerlund F (2016a) Direct identification of antibiotic resistance genes on single plasmid molecules using CRISPR/Cas9 in combination with optical DNA mapping. *Scientific Reports* **6**, 37938.
- Müller V, Karami N, Nyberg LK, Pichler C, Torche Pedreschi PC, Quaderi S, Fritzsche J, Ambjörnsson T, Åhrén C and Westerlund F (2016b) Rapid tracing of resistance plasmids in a nosocomial outbreak using optical DNA mapping. *ACS Infectious Diseases* **2**, 322–328.
- Müller V, Dvirnas A, Andersson J, Singh V, Sriram KK, Johansson P, Ebenstein Y, Ambjörnsson T and Westerlund F (2019) Enzyme-free optical DNA mapping of the human genome using competitive binding. *Nucleic Acids Research* **47**, e89.
- Müller V, Nyblom M, Johnning A, Wrände M, Dvirnas A, Sriram KK, Giske CG, Ambjörnsson T, Sandegren L, Kristiansson E and Westerlund F (2020) Cultivation-free typing of bacteria using optical DNA mapping. *ACS Infectious Diseases* **6**, 1076–1084.
- Muralidhar A and Dorfman KD (2016) Backfolding of DNA confined in nanotubes: flory theory versus the two-state cooperativity model. *Macromolecules* **49**, 1120–1126.
- Muralidhar A, Tree DR and Dorfman KD (2014a) Backfolding of wormlike chains confined in nanochannels. *Macromolecules* **47**, 8446–8458.

- Muralidhar A, Tree DR, Wang Y and Dorfman KD (2014b) Interplay between chain stiffness and excluded volume of semiflexible polymers confined in nanochannels. *Journal of Chemical Physics* **140**, 084905.
- Muralidhar A, Quevillon MJ and Dorfman KD (2016) The backfolded odijk regime for wormlike chains confined in rectangular nanochannels. *Polymers* **8**, 8030079.
- Neely RK, Deen J and Hofkens J (2011) Optical mapping of DNA: single-molecule-based methods for mapping genomes. *Biopolymers* **95**, 298–311.
- Nilsson AN, Emilsson G, Nyberg LK, Noble C, Stadler LS, Fritzsche J, Moore ERB, Tegenfeldt JO, Ambjörnsson T and Westerlund F (2014) Competitive binding-based optical DNA mapping for fast identification of bacteria – multi-ligand transfer matrix theory and experimental applications on *Escherichia coli*. *Nucleic Acids Research* **42**, e118.
- Noding B and Koster S (2012) Intermediate filaments in small configuration spaces. *Physical Review Letters* **108**, 088101.
- Nyberg LK, Persson F, Berg J, Bergström J, Fransson E, Olsson L, Persson M, Stålnacke A, Wigenius J, Tegenfeldt JO and Westerlund F (2012) A single-step competitive binding assay for mapping of single DNA molecules. *Biochemical and Biophysical Research Communications* **417**, 404–408.
- Nyberg L, Persson F, Akerman B and Westerlund F (2013) Heterogeneous staining: a tool for studies of how fluorescent dyes affect the physical properties of DNA. *Nucleic Acids Research* **41**, e184.
- Nyberg LK, Quaderi S, Emilsson G, Karami N, Lagerstedt E, Müller V, Noble C, Hammarberg S, Nilsson AN, Sjöberg F, Fritzsche J, Kristiansson E, Sandegren L, Ambjörnsson T and Westerlund F (2016) Rapid identification of intact bacterial resistance plasmids via optical mapping of single DNA molecules. *Scientific Reports* **6**, 30410.
- Odijk T (1977) Polyelectrolytes near the rod limit. *Journal of Polymer Science: Polymer Physics Edition* **15**, 477–483.
- Odijk T (1983) The statistics and dynamics of confined or entangled stiff polymers. *Macromolecules* **16**, 1340–1344.
- Odijk T (2006) DNA confined in nanochannels: hairpin tightening by entropic depletion. *Journal of Chemical Physics* **125**, 204904.
- Odijk T (2008) Scaling theory of DNA confined in nanochannels and nanoslits. *Physical Review E* **77**, 060901.
- Odman D, Werner E, Dorfman KD, Doering CR and Mehlig B (2018) Distribution of label spacings for genome mapping in nanochannels. *Biomicrofluidics* **12**, 034115.
- Orlandini E and Micheletti C (2013) Knotting of linear DNA in nano-slits and nano-channels: a numerical study. *Journal of Biological Physics* **39**, 267–275.
- Öz R, Sriram KK and Westerlund F (2019) A nanofluidic device for real-time visualization of DNA-protein interactions on the single DNA molecule level. *Nanoscale* **11**, 2071–2078.
- Öz R, Howard SM, Sharma R, Törnkvist H, Ceppi I, Sriram KK, Kristiansson E, Cejka P and Westerlund F (2020) Phosphorylated CIP bridges DNA to promote annealing of broken ends. *Proceedings of the National Academy of Sciences of the USA* **117**, 21403.
- Öz R, Wang JL, Guerois R, Goyal G, Sriram KK, Ropars V, Sharma R, Koca F, Charbonnier J-B, Modesti M, Strick TR and Westerlund F (2021) Dynamics of Ku and bacterial non-homologous end-joining characterized using single DNA molecule analysis. *Nucleic Acids Research* **49**, 2629–2641.
- Park Y-S, Oh JM and Cho Y-K (2018) Non-lithographic nanofluidic channels with precisely controlled circular cross sections. *RSC Advances* **8**, 19651–19658.
- Perkins TT, Smith DE, Larson RG and Chu S (1995) Stretching of a single tethered polymer in a uniform flow. *Science* **268**, 83–87.
- Persson F, Utiko P, Reisner W, Larsen NB and Kristensen A (2009) Confinement spectroscopy: probing single DNA molecules with tapered nanochannels. *Nano Letters* **9**, 1382–1385.
- Persson F, Fritzsche J, Mir KU, Modesti M, Westerlund F and Tegenfeldt JO (2012) Lipid-based passivation in nanofluidics. *Nano Letters* **12**, 2260–2265.
- Polson JM (2018) Free energy of a folded semiflexible polymer confined to a nanochannel of various geometries. *Macromolecules* **51**, 5962–5971.
- Polson JM and Hastie CG (2020) Free energy of a knotted polymer confined to narrow cylindrical and conical channels. *Physical Review E* **102**, 052502.
- Randall GC and Doyle PS (2005) DNA deformation in electric fields: DNA driven past a cylindrical obstruction. *Macromolecules* **38**, 2410–2418.
- Reginato G and Cejka P (2020) The MRE11 complex: a versatile toolkit for the repair of broken DNA. *DNA Repair* **91–92**, 102869.
- Reifenberger JG, Cao H and Dorfman KD (2018) Odijk excluded volume interactions during the unfolding of DNA confined in a nanochannel. *Macromolecules* **51**, 1172–1180.
- Reinhart WF, Tree DR and Dorfman KD (2013) Entropic depletion of DNA in triangular nanochannels. *Biomicrofluidics* **7**, 024102.
- Reinhart WF, Reifenberger JG, Gupta D, Muralidhar A, Sheats J, Cao H and Dorfman KD (2015) Distribution of distances between DNA barcode labels in nanochannels close to the persistence length. *The Journal of Chemical Physics* **142**, 064902.
- Reisner W, Morton KJ, Riehn R, Wang YM, Yu Z, Rosen M, Sturm JC, Chou SY, Frey E and Austin RH (2005) Statics and dynamics of single DNA molecules confined in nanochannels. *Physical Review Letters* **94**, 196101.
- Reisner W, Beech JP, Larsen NB, Flyvbjerg H, Kristensen A and Tegenfeldt JO (2007) Nanoconfinement-enhanced conformational response of single DNA molecules to changes in ionic environment. *Physical Review Letters* **99**, 058302.
- Reisner W, Larsen NB, Silaharoglu A, Kristensen A, Tommerup N, Tegenfeldt JO and Flyvbjerg H (2010) Single-molecule denaturation mapping of DNA in nanofluidic channels. *Proceedings of the National Academy of Sciences of the USA* **107**, 13294–13299.
- Reisner W, Pedersen JN and Austin RH (2012) DNA confinement in nanochannels: physics and biological applications. *Reports on Progress in Physics* **75**, 106601.
- Riehn R, Lu MC, Wang YM, Lim SF, Cox EC and Austin RH (2005) Restriction mapping in nanofluidic devices. *Proceedings of the National Academy of Sciences of the USA* **102**, 10012–10016.
- Roushan M, Kaur P, Karpusenka A, Countryman PJ, Ortiz CP, Fang Lim S, Wang H and Riehn R (2014) Probing transient protein-mediated DNA linkages using nanoconfinement. *Biomicrofluidics* **8**, 034113.
- Roushan M, Azad Z, Movahed S, Ray PD, Livshits GI, Lim SF, Weninger KR and Riehn R (2018) Motor-like DNA motion due to an ATP-hydrolyzing protein under nanoconfinement. *Scientific Reports* **8**, 10036.
- Schaefer DW, Joanny JF and Pincus P (1980) Dynamics of semiflexible polymers in solution. *Macromolecules* **13**, 1280–1289.
- Schmitt A, Jiang K, Camacho MI, Jonna VR, Hofer A, Westerlund F, Christie PJ and Berntsson RP (2018) PrgB promotes aggregation, biofilm formation, and conjugation through DNA binding and compaction. *Molecular Microbiology* **109**, 291–305.
- Schotzinger RM, Menard LD and Ramsey JM (2020) Single-molecule DNA extension in rectangular and square profile nanochannels in the extended de Gennes regime. *Macromolecules* **53**, 1950–1956.
- Schwartz DC, Li X, Hernandez LI, Ramnarain SP, Huff EJ and Wang YK (1993) Ordered restriction maps of *Saccharomyces cerevisiae* chromosomes constructed by optical mapping. *Science* **262**, 110–114.
- Scott S, Xu ZM, Kouzine F, Berard DJ, Shaheen C, Gravel B, Saunders L, Hofkirchner A, Leroux C, Laurin J, Levens D, Benham CJ and Leslie SR (2018) Visualizing structure-mediated interactions in supercoiled DNA molecules. *Nucleic Acids Research* **46**, 4622–4631.
- Scott S, Shaheen C, McGuinness B, Metera K, Kouzine F, Levens D, Benham CJ and Leslie S (2019) Single-molecule visualization of the effects of ionic strength and crowding on structure-mediated interactions in supercoiled DNA molecules. *Nucleic Acids Research* **47**, 6360–6368.
- Shaheen C, Hastie C, Metera K, Scott S, Zhang Z, Chen S, Gu G, Weber L, Munsky B, Kouzine F, Levens D, Benham C and Leslie S (2022) Non-equilibrium structural dynamics of supercoiled DNA plasmids exhibits asymmetrical relaxation. *Nucleic Acids Research* **50**, 2754–2764.
- Sharim H, Grunwald A, Gabrieli T, Michaeli Y, Margalit S, Torchinsky D, Ariely R, Nifker G, Juhasz M, Gularek F, Almalvez M, Dufault B, Chandra SS, Liu A, Bhattacharya S, Chen YW, Vilain E, Wagner KR, Pevsner J, Reifenberger J, Lam ET, Hastie AR, Cao H, Barseghyan H, Weinhold E and Ebenstein Y (2019) Long-read single-molecule maps of the functional methylome. *Genome Research* **29**, 646–656.
- Sharma R, Sriram KK, Holmstrom ED and Westerlund F (2020) Real-time compaction of nanoconfined DNA by an intrinsically disordered macromolecular counterion. *Biochemical and Biophysical Research Communications* **533**, 175–180.

- Sheats J, Reifengerger JG, Cao H and Dorfman KD** (2015) Measurements of DNA barcode label separations in nanochannels from time-series data. *Biomicrofluidics* **9**, 064119.
- Skolnick J and Fixman M** (1977) Electrostatic persistence length of a worm-like polyelectrolyte. *Macromolecules* **10**, 944–948.
- Smith TSC, Iarko V, Muralidhar A, Werner E, Dorfman KD and Mehlig B** (2015) Finite-size corrections for confined polymers in the extended de Gennes regime. *Physical Review E* **92**, 062601.
- Stigter D** (1975) The charged colloidal cylinder with a gouy double layer. *Journal of Colloid and Interface Science* **53**, 296–306.
- Stigter D** (1977) Interactions of highly charged colloidal cylinders with applications to double-stranded DNA. *Biopolymers* **16**, 1435–1448.
- Streng DE, Lim SF, Pan J, Karpusenko A and Riehn R** (2009) Stretching chromatin through confinement. *Lab on a Chip* **9**, 2772–2774.
- Su T, Das SK, Xiao M and Purohit PK** (2011) Transition between two regimes describing internal fluctuation of DNA in a nanochannel. *PLoS ONE* **6**, e16890.
- Suma A, Orlandini E and Micheletti C** (2015) Knotting dynamics of DNA chains of different length confined in nanochannels. *Journal of Physics: Condensed Matter* **27**, 354102.
- Tan CJ, Basak R, Yadav I, van Kan JA, Arluison V and van der Maarel JRC** (2022) Mobility of bacterial protein Hfq on dsDNA: role of C-terminus-mediated transient binding. *The Journal of Physical Chemistry B* **126**, 1477–1482.
- Tegenfeldt JO, Prinz C, Cao H, Chou S, Reisner WW, Riehn R, Wang YM, Cox EC, Sturm JC, Silberzan P and Austin RH** (2004) The dynamics of genomic-length DNA molecules in 100-nm channels. *Proceedings of the National Academy of Sciences of the USA* **101**, 10979–10983.
- Thamdrup LHE, Klukowska A and Kristensen A** (2008) Stretching DNA in polymer nanochannels fabricated by thermal imprint in PMMA. *Nanotechnology* **19**, 125301.
- Tisi R, Vertemara J, Zampella G and Longhese MP** (2020) Functional and structural insights into the MRX/MRN complex, a key player in recognition and repair of DNA double-strand breaks. *Computational and Structural Biotechnology Journal* **18**, 1137–1152.
- Torchinsky D, Michaeli Y, Gassman NR and Ebenstein Y** (2019) Simultaneous detection of multiple DNA damage types by multi-colour fluorescent labelling. *Chemical Communications* **55**, 11414–11417.
- Torstensson E, Goyal G, Johnning A, Westerlund F and Ambjörnsson T** (2021) Combining dense and sparse labeling in optical DNA mapping. *PLoS ONE* **16**, e0260489.
- Tree DR, Muralidhar A, Doyle PS and Dorfman KD** (2013a) Is DNA a good model polymer? *Macromolecules* **46**, 8369–8382.
- Tree DR, Wang Y and Dorfman KD** (2013b) Extension of DNA in a nanochannel as a rod-to-coil transition. *Physical Review Letters* **110**, 208103.
- Trizac E and Shen T** (2016) Bending stiff charged polymers: the electrostatic persistence length. *EPL (Europhysics Letters)* **116**, 18007.
- Uba FI, Pullagurra SR, Sirasunthorn N, Wu J, Park S, Chantiwas R, Cho Y-K, Shin H and Soper SA** (2015) Surface charge, electroosmotic flow and DNA extension in chemically modified thermoplastic nanoslits and nanochannels. *The Analyst* **140**, 113–126.
- Uppuluri L, Jadhav T, Wang Y and Xiao M** (2021) Multicolor whole-genome mapping in nanochannels for genetic analysis. *Analytical Chemistry* **93**, 9808–9816.
- Utiko P, Persson F, Kristensen A and Larsen NB** (2011) Injection molded nanofluidic chips: fabrication method and functional tests using single-molecule DNA experiments. *Lab on a Chip* **11**, 303–308.
- van Kan JA, Zhang C, Perumal Malar P and van der Maarel JR** (2012) High throughput fabrication of disposable nanofluidic lab-on-chip devices for single molecule studies. *Biomicrofluidics* **6**, 36502.
- Wang Z-G** (2017) 50th Anniversary perspective: polymer conformation – a pedagogical review. *Macromolecules* **50**, 9073–9114.
- Wang YM, Tegenfeldt JO, Reisner W, Riehn R, Guan XJ, Guo L, Golding I, Cox EC, Sturm J and Austin RH** (2005) Single-molecule studies of repressor-DNA interactions show long-range interactions. *Proceedings of the National Academy of Sciences of the USA* **102**, 9796–9801.
- Wang Y, Tree DR and Dorfman KD** (2011) Simulation of DNA extension in nanochannels. *Macromolecules* **44**, 6594–6604.
- Wang C, Bruce RL, Duch EA, Patel JV, Smith JT, Astier Y, Wunsch BH, Meshram S, Galan A, Scerbo C, Pereira MA, Wang D, Colgan EG, Lin Q and Stolovitzky G** (2015) Hydrodynamics of diamond-shaped gradient nanopillar arrays for effective DNA translocation into nanochannels. *ACS Nano* **9**, 1206–1218.
- Welch RL, Sladek R, Dewar K and Reisner WW** (2012) Denaturation mapping of *Saccharomyces cerevisiae*. *Lab on a Chip* **12**, 3314–3321.
- Werner E and Mehlig B** (2014) Confined polymers in the extended de Gennes regime. *Physical Review E* **90**, 062602.
- Werner E and Mehlig B** (2015) Scaling regimes of a semiflexible polymer in a rectangular channel. *Physical Review E* **91**, 050601.
- Werner E, Persson F, Westerlund F, Tegenfeldt JO and Mehlig B** (2012) Orientational correlations in confined DNA. *Physical Review E* **86**, 041802.
- Werner E, Cheong GK, Gupta D, Dorfman KD and Mehlig B** (2017) One-parameter scaling theory for DNA extension in a nanochannel. *Physical Review Letters* **119**, 268102.
- Werner E, Jain A, Muralidhar A, Frykholm K, St Clere Smithe T, Fritzsche J, Westerlund F, Dorfman KD and Mehlig B** (2018) Hairpins in the conformations of a confined polymer. *Biomicrofluidics* **12**, 024105.
- Westerlund F, Persson F, Fritzsche J, Beech JP and Tegenfeldt JO** (2018) Fluorescence microscopy of nanochannel-confined DNA. In Peterman EJG (ed.), *Single Molecule Analysis: Methods and Protocols*. New York, NY: Springer New York, pp. 173–198.
- Wilkinson OJ, Martín-González A, Kang H, Northall SJ, Wigley DB, Moreno-Herrero F and Dillingham MS** (2019) CIP forms a tetrameric dumbbell-shaped particle which bridges complex DNA end structures for double-strand break repair. *eLife* **8**, e42129.
- Wu J, Chantiwas R, Amirsadeghi A, Soper SA and Park S** (2011) Complete plastic nanofluidic devices for DNA analysis via direct imprinting with polymer stamps. *Lab on a Chip* **11**, 2984–2989.
- Wu S, Turner KM, Nguyen N, Raviram R, Erb M, Santini J, Luebeck J, Rajkumar U, Diao Y, Li B, Zhang W, Jameson N, Corces MR, Granja JM, Chen X, Coruh C, Abnoui A, Houston J, Ye Z, Hu R, Yu M, Kim H, Law JA, Verhaak RGW, Hu M, Furnari FB, Chang HY, Ren B, Bafna V and Mischel PS** (2019) Circular ecDNA promotes accessible chromatin and high oncogene expression. *Nature* **575**, 699–703.
- Yadav I, Basak R, Yan P, van Kan JA, Arluison V and van der Maarel JRC** (2020) Role of internal DNA motion on the mobility of a nucleoid-associated protein. *The Journal of Physical Chemistry Letters* **11**, 8424–8429.
- Yang Y, Burkhardt TW and Gompper G** (2007) Free energy and extension of a semiflexible polymer in cylindrical confining geometries. *Physical Review E* **76**, 011804.
- Young E, Abid HZ, Kwok P-Y, Riethman H and Xiao M** (2020) Comprehensive analysis of human subtelomeres by whole genome mapping. *PLoS Genetics* **16**, e1008347.
- Zhang C, Zhang F, Kan JAV and Maarel JRCVD** (2008) Effects of electrostatic screening on the conformation of single DNA molecules confined in a nanochannel. *The Journal of Chemical Physics* **128**, 225109.
- Zhang C, Shao PG, Kan JAV and Maarel JRCVD** (2009) Macromolecular crowding induced elongation and compaction of single DNA molecules confined in a nanochannel. *Proceedings of the National Academy of Sciences of the USA* **106**, 16651–16656.
- Zhang C, Gong Z, Guttula D, Malar PP, van Kan JA, Doyle PS and van der Maarel JR** (2012) Nanofluidic compaction of DNA by like-charged protein. *Journal of Physical Chemistry B* **116**, 3031–3036.
- Zhang C, Guttula D, Liu F, Malar PP, Ng SY, Dai L, Doyle PS, van Kan JA and van der Maarel JRC** (2013a) Effect of H-NS on the elongation and compaction of single DNA molecules in a nanospace. *Soft Matter* **9**, 9593–9601.
- Zhang C, Jiang K, Liu F, Doyle PS, van Kan JA and van der Maarel JR** (2013b) A nanofluidic device for single molecule studies with *in situ* control of environmental solution conditions. *Lab on a Chip* **13**, 2821–2826.
- Zhang D, Chan S, Sugerman K, Lee J, Lam ET, Bocklandt S, Cao H and Hastie AR** (2018) CRISPR-bind: a simple, custom CRISPR/dCas9-mediated labeling of genomic DNA for mapping in nanochannel arrays. *bioRxiv*, 371518. <https://doi.org/10.1101/371518>.
- Zirkin S, Fishman S, Sharim H, Michaeli Y, Don J and Ebenstein Y** (2014) Lighting up individual DNA damage sites by *in vitro* repair synthesis. *Journal of the American Chemical Society* **136**, 7771–7776.